SELECTED ELECTRICAL PROPERTIES OF R.F. SPUTTERED Al_2O_3-Cr_2O_3 THIN FILMS

A THESIS

Presented to

The Faculty of the Division of Graduate

Studies and Research

By

Bryant Coffin Bechtold

In Partial Fulfillment

of the Requirements for the Degree

Master of Science in Ceramic Engineering

Georgia Institute of Technology

March, 1975

SELECTED ELECTRICAL PROPERTIES

OF R.F. SPUTTERED Al_2O_3-Cr_2O_3 THIN FILMS

Approved:

Joe K. Cochran, Jr. Chairman

James F. Benzel

Alan T. Chapman

Date approved by Chairman 2-28-75

ACKNOWLEDGEMENTS

Sincere appreciation and thanks are extended to Dr. Joe K. Cochran for his advice, willingness to assist, patience and constant encouragement throughout the entire scope of this investigation. Gratitude is also offered to Mr. Thomas Mackrovitch for his help in fabricating several vital pieces of equipment and to Drs. Alan T. Chapman and James F. Benzel for taking their valuable time to serve on the reading committee.

My appreciation is also extended to two special people--my mother, for her willingness to do such a masterful job of typing in such a short amount of time, and my wife Janet, whose constant love, encouragement and fortitude during the writing of this thesis helped me overcome any problems encountered.

TABLE OF CONTENTS

TABLE OF CONTENTS (Continued)

LIST OF TABLES

LIST OF ILLUSTRATIONS

LIST OF ILLUSTRATIONS (Continued)

SUMMARY

Selected electrical properties were investigated in polycrystalline $Al_{2-x}Cr_xO_3$ thin films r.f. sputtered from solid solution targets consisting of 0, 4.1, 7.8, 11.8, 14.6 and 19.0 mole percent Cr_2O_3. The films were deposited in a temperature range of 350-450°C and shown to possess both long-range and short-range order with crystal structures similar to cubic γ-Al_2O_3 by electron diffraction studies. Relative chromium contents in the films were proportional to the chromium contents of the targets but absolute chromium contents were not determined.

Average resistivities ($\cong 5 \times 10^{14}$ ohm-cm) and dielectric strengths ($\cong 6 \times 10^6$ volts/cm) of films 1200-2600 A thick were found to vary approximately one order of magnitude for the composition range studied. Current-voltage relationships in the films indicated that two types of conduction mechanism existed in the $Al_{2-x}Cr_xO_3$ films. At high applied electric fields, all compositions studied exhibited conduction that varied exponentially with the square root of the applied electric field. At lower applied electric fields, conduction exhibiting ohmic characteristics existed in the 4.1 and 19.0 mole percent Cr_2O_3 films.

CHAPTER I

INTRODUCTION

In recent years, advances in thin film technology have made possible great strides in the solid state electronics field. Due to better methods of dielectric thin film deposition, such as r.f. (radio frequency) sputtering, integrated microcircuits have greatly improved. Thin insulating films are utilized in integrated and hybrid microcircuits as capacitor dielectrics, diffusion masks, gate insulators for metal-insulator semiconductor field effect devices, for surface passivation, and as insulators between layers of conductive films used for interconnections. Quite naturally, electrical properties and characteristics of thin insulating films used in such devices are quite important.

The purpose of this investigation was to study selected electrical properties--resistivity, dielectric strength, current-voltage relationships--of r.f. sputtered $Al_{2-x}Cr_xO_3$ thin insulating films. Increasing mole percent additions of Cr_2O_3 to Al_2O_3 should lower the resistivity of the thin films. Dielectric strengths of the $Al_{2-x}Cr_xO_3$ thin films were measured to determine what voltages could be applied without destroying the insulating film. Current-voltage relationships were also investigated to study possible conduction mechanisms in the films.

CHAPTER II

A SURVEY OF THE LITERATURE

A review of the literature on radio frequency (r.f.) sputtering as a method of thin film preparation is presented in this Chapter. Included is the theory of r.f. sputtering, parameters affecting the r.f. sputtering of thin films, properties of r.f. sputtered thin films, and the advantages and disadvantages of r.f. sputtering over other types of thin film preparation methods. Various conduction mechanisms in thin insulating films are also discussed. This Chapter ends with a presentation of the physical and electrical properties of the Al_2O_3-Cr_2O_3 system.

R.F. Sputtering

Theory

Bombarding the surface of a material with molecules, atoms or ions can cause many interesting phenomena to occur.[1] If the kinetic energy of these bombarding particles exceeds the binding energy of the atoms (the binding energy is related to the heat of sublimation of a material) in the bombarded material, the atoms of the lattice will be pushed into new positions, resulting in both surface migration of atoms and surface damage. If these bombarding particles exhibit kinetic energies approaching four times the heat of sublimation of the bombarded material, atoms on the surface of the bombarded material will be ejected into the surrounding gas phase. The ejection of atoms from the

surface of a material through the bombarding of particles is known as physical sputtering. Since high-energy ion beams can readily be produced and accelerated to the required kinetic energies by electric fields, ions are used instead of atoms or molecules as the bombarding particles.

When the bombarding ions strike the surface to be sputtered, the energy of the ions is transferred to the bombarded surface in the area of impact. Thus, the basic mechanism of the ejection of the surface material is momentum transfer,[2] with other complex second-order phenomena. Those ions that penetrate the surface of the target give up their energy by vibrating the lattice and these same ions will not participate in the removal of material unless the sputtered material is volatile, causing sublimation. Ions that do not penetrate the surface uniformly strip a layer of material from the bombarded surface, without a change in chemical composition.

The most common way to sputter a material is to let the material being sputtered serve as the cathode in a low pressure dc glow discharge.[3] Since almost the entire glow discharge is dropped across the ion sheath that surrounds the cathode (Crookes dark space), the cathode will be under steady bombardment by high-energy ions and consequently, it will be sputtered. This ion sheath is formed because the target potential is negative with respect to the plasma, and electrons are forced away from the surface. This technique is applicable only to conductors.

When insulators, such as many of the metal oxides, are used, the accelerating potential cannot be directly applied to the insulator, and

the positive charge which accumulates on the surface during ion bombardment cannot be neutralized. Thus, a dc glow discharge cannot be started. This can be overcome by applying a high frequency potential, such as radio frequency, to a metal electrode behind the insulator. By capacitive coupling through the insulator, an r.f. voltage is induced on the front surface of the insulator.[4] The insulator will then be alternately ion bombarded and electron bombarded,[3] with the positive charge that accumulates on the surface during the negative or sputter portion of each cycle being neutralized by electrons during the positive part of each cycle. A schematic of the set-up is shown in Figure 1.

Since electron mobility is several orders of magnitude greater than that of positive ion mobility,[3] more electrons are attracted to the insulator during the positive half of the cycle than are ions during the negative half of the cycle. Thus, the insulator surface will self-bias negatively with respect to the plasma; if this was not the case, an excessive electron current would flow to the insulator during each cycle. Since the insulator potential is negative with respect to the plasma, electrons are repelled by the insulator surface, and an ion sheath forms that is visible as a dark space near the insulator surface.[2]

The frequency of the applied voltage must be at least 10^6 Hz to prevent excessive positive charge accumulation at the insulator surface.[2] If the frequency is too low, enough ions reach the insulator surface during the negative half of the cycle to neutralize the negative surface charge and no dc potential will build up. The lowest frequency at which ion sheath formation occurs[3] is of the order 10^3 Hz.

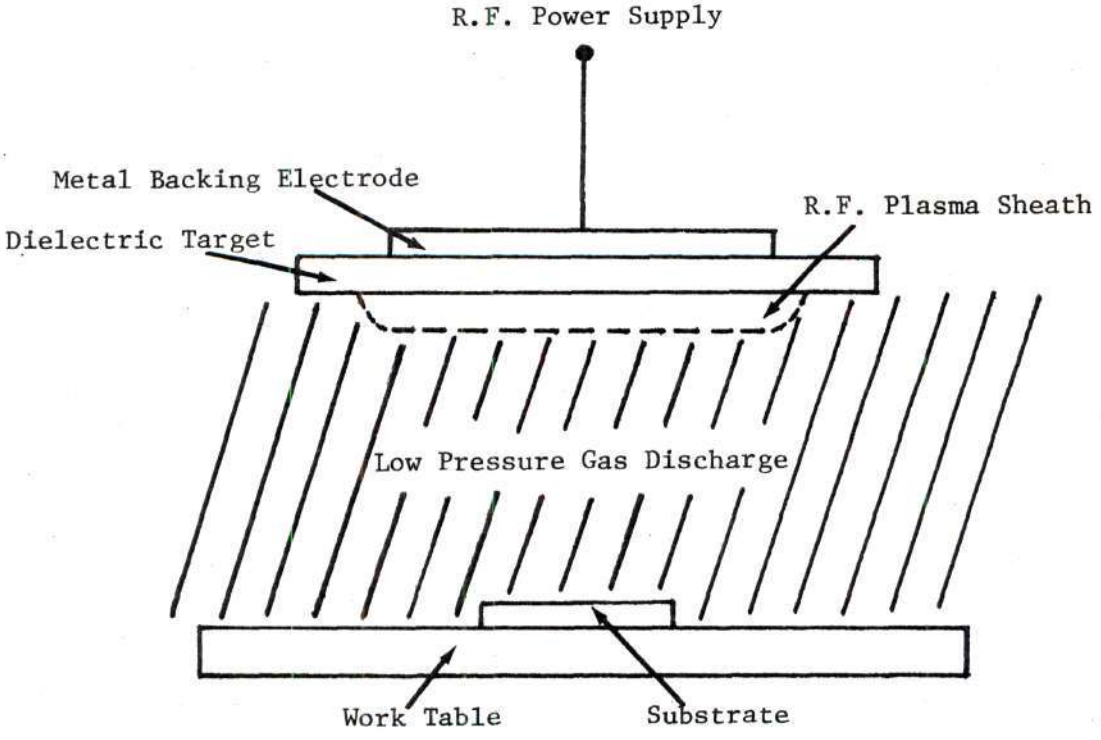

Figure 1. Setup During R.F. Sputtering of a Dielectric. (After Jackson.[4])

Higher frequencies result in fewer ions reaching the insulator surface, thereby increasing the negative bias which creates an increased potential across the dark space and increases sputtering rates.

Parameters Affecting Sputtering Process

The part of the sputtering process which is usually affected by changing conditions is the deposition rate of the thin film. Other portions of the sputtering process which can be affected include the glow discharge and properties of the deposited films such as composition and uniformity in thickness.

The discharge gas most commonly used for sputtering is argon because of its availability in high purity form, its high atomic weight and its inertness. Gases such as oxygen require a great deal of energy to sustain a glow discharge,[2] thereby reducing the energy available to the positive ions used in the sputtering process. Consequently, deposition rates in pure oxygen are about half those in argon. Davidse and Maissel[3] found that the sputtering rate falls off sharply with the addition of small percentages of O_2 gas to the sputtering gas argon when r.f. sputtering dielectric materials. At higher concentrations of O_2 gas, the rate did not vary much until the O_2 gas percent exceeded 50 percent, where the glow discharge became unstable. Maissel and Glang[1] state that gaseous impurities in argon can cause a reduction in the deposition rate.

Vossen and O'Neill[2] found the deposition rate to be unaffected in the pressure range between 2×10^{-3} and 15×10^{-3} torr. Above 15×10^{-3} torr, the deposition rate decreased rapidly with increasing pressure.

The use of an auxiliary magnetic field has a number of effects on the sputtering process. Such a field will not only result in a more well defined glow discharge,[3] but it will also increase the deposition rate. In addition, the glow discharge can be maintained at lower pressures[2] and the turbulence added to the discharge improves the uniformity of film thickness over large substrate areas.

In studying the size and shape of the electrode, Davidse and Maissel[3] found that more power was needed for a square electrode than for a circular electrode to obtain the same deposition rate at constant pressure due to loss of power at the corners of the square electrode. Increasing the electrode diameter from 12.5 to 19 cm resulted in lowering the r.f. potential needed to produce a given deposition rate.

In general, sputtering rates will decrease with an increase in target thickness, the best target thickness being 0.3 to 0.7 cm. The target-substrate separation distance is also fairly critical.[2] Separation cannot be less than or equal to the ion sheath thickness if the glow discharge is to be initiated and maintained. A reasonable separation is 2.5 to 3.0 cm. The substrate temperature will also control the deposition rate;[3] the deposition rate for a cooled substrate is twice as fast as that for a substrate at 500^{o}C. A uniform substrate temperature is imperative for uniform film thickness.

Changes in the r.f. voltage, current, or power will also affect the sputtering process.[2] An increase in any of the three will increase the deposition rate.

Properties of R.F. Sputtered Films

In sputtering, momentum transfer from the fast-moving positive ions attracted from the discharge toward the target (insulator) surface causes disintegration of the target surface by rupturing surface bonds. The material transferred from the target to the vapor state has the same composition after reaching equilibrium conditions. But, most of the molecules are probably dissociated in the sputtering process and thus the material arriving at the substrate is in predominantly atomic form.[1] It has not been determined whether low-energy noble-gas ion bombardment, the high kinetic energies of the sputtered atoms, or other phenomena provide the activation energies needed to reassemble the atoms back into the proper molecules. In general, the composition of the film is almost identical to that of the sputtered material.

During sputtering of such compounds as oxides, the energy involved in the collisions between the ions and ejected target material may be enough to exceed the chemical bonding energy. Thus, oxygen could preferentially leave the target, resulting in an oxygen deficient target. Wehner et al.,[5] in studying Hg-ion bombarded oxide powders, found CuO to be reduced to Cu_2O and then to Cu and Fe_2O_3 to be reduced to Fe_3O_4 to FeO and finally to Fe. Oxygen deficiencies in sputtered Corning 1715 glass were found by Pliskin[6] in his study of thin film insulators.

Vossen and O'Neill[2] offered two possible mechanisms for the non-stoichiometric behavior of the thin film: (1) the argon discharge can chemically reduce cyrstalline oxides of low chemical bond strength, and

(2) sublimation may occur from the target or substrate when one of the constituents is highly volatile. They group insulators into three groups--simple crystalline oxides such as SiO_2 or Al_2O_3; multicomponent solids such as $BaTiO_3$ or $2CdO \cdot Nb_2O_5$; and noncrystalline solids. Crystalline oxides were listed according to their ease of reduction by using their heat of dissociation of the oxygen atom as the determining factor (see Table 1). At discharge voltages of 3600 volts, molecules with dissociation energies less than or equal to that of ZrO_2 (129.2 kcal/mole) were found to reduce partially, whereas any oxide having a dissociation energy higher than that of SrO (141.2 kcal/mole) did not reduce. Multicomponent crystalline materials also exhibited problems with stoichiometry due to one or more volatile constituents. In studying $Cd_xNb_2O_{5+x}$ a decrease in the Cd content was noted with increased target usage. If an oxide is likely to reduce, one method to overcome this problem is to sputter with an argon-oxygen mixture to replenish the oxygen.

Davidse and Maissel[3] cite uneven temperature distribution in the target material as another possible cause for the variation in chemical composition of a sputtered film. If the target is not uniform in composition and properties, then the temperature will be higher in some regions than in others. This can lead to hot spots in the target at high power densities, resulting in nonuniform sputtering rates and sometimes in a variation in chemical composition across the film.

The r.f. sputtered films are generally uniform in thickness and composition.[2] The structure of the film depends primarily on the

Table 1. Dissociation Energy per Oxygen Atom for Selected Oxides (After Vossen and O'Neill[2])

Molecule	Heat of Dissociation Oxygen Atom kcal/mole
Cr_2O_3	89.8
Nb_2O_5	92.64
TiO_2	109.0
ZrO_2	129.2
BaO	133.4
SrO	141.2
CaO	151.8
La_2O_3	152.5
SiO_2	153.9
Al_2O_3	195.9

deposition rate and substrate temperature. Dielectric films deposited at rates below 200 Å/min usually exhibit a noncrystalline or amorphous structure. In addition, the films do not have theoretical density. Heating either during or after deposition can crystallize the film, but heating the substrate during deposition reduces the deposition rate. Dielectric properties of the films deposited at high rates will approach the bulk properties of the composition upon heating.

Toughness and good adhesion are other properties of r.f. sputtered films. Davidse[7] attributes the good adhesion to the relatively high energies of the sputtered species and the continuous cleaning of the surface by the glow discharge. Vossen and O'Neill[2] state that good adhesion results from the high arrival energy of the sputtered material at the substrate and the chemical bonding that can exist at the film-substrate interface. MacDonald and Haneman[8] have shown that many sputtered atoms have sufficient energy to penetrate one to two atomic layers into the surface on which they land, thus leading to a film with good adhesion to the substrate.

Advantages and Disadvantages of R.F. Sputtering

Advantages of r.f. sputtering over other methods of film deposition include:[1,2]

1. R.f. sputtering is extremely versatile. In theory, any material can be deposited as a thin film by r.f. sputtering.

2. Precise control of film thickness and deposition rate can be achieved.

3. Uniformity of film thickness and stoichiometry over large substrate areas in many cases are excellent.

4. Deposited films usually have excellent mechanical properties such as adhesion.

5. It is an atom-by-atom process resulting in nonporous films with surfaces closely reproducing the substrate surface.

Disadvantages of r.f. sputtering include:

1. Deposition rates are slow.

2. The basic process mechanism is complex.

Conduction Mechanisms through Thin Insulating Films

Resistivity can be used as a measure of the ability of a material to pass an electric current. The higher the resistivity, the more difficult it is to pass an electric current through the material. The resistivity, ρ, in ohm-centimeters, of a material can be calculated by the equation[18]

$$\rho = \frac{RA}{\ell} \tag{1}$$

where R is the resistance of the material in ohms, A is the area in cm^2 and ℓ is the length or thickness in cm. Insulators are materials which have very few mobile charge carriers available to pass an electric current under an applied field and are characterized by resistivities greater than 10^{12} ohm-cm^{12}. On the other hand, conductors are materials which have large numbers of mobile charge carriers and thus lower resistivities, on the order of 10^{-6} ohm-cm. Semiconductors exhibit electrical conductivities intermediate between insulators and conductors and possess resistivities in the range 10^{-3} to 10^{9} ohm-cm. Thin film resistivities are of major importance in many electronic circuits.

A property important in thin films utilized for electronic circuits is breakdown voltage, from which the dielectric strength of the film can be calculated. Gerstenberg,[1] assuming that the dielectric strength is independent of film thickness, states

$$V_D = E_D d \tag{2}$$

where V_D is the breakdown voltage in volts, E_D is the dielectric breakdown strength in volts/cm and d is the dielectric thickness in cm. Kingery[12] states that in general, as sample thickness decreases, measured dielectric strength increases. Dielectric strength refers to the material's ability to prevent the passage of current.[19] Subjection of the thin film to an intense voltage gradient may result in a strain due to the field forces on the ions and electrons which exceeds the dielectric strength and the dielectric film will begin to break down, allowing the passage of current. In thin films, breakdown is more typically due to flaws rather than intrinsic behavior.[1] Breakdown might originate at pinholes, voids and defects in the film caused by dust on the substrate or by some local inhomogeneity.

When working with thin films, applying a bias of only a few volts will induce electric fields on the order of 10^4 or 10^5 volts/cm; thus, the study of conduction mechanisms in thin films is centered around high-field electrical properties of the thin films. Quite often, high-field electrical properties cannot be adequately described by a single conduction process[1] since various field-strength ranges might exhibit different electrical behavior. Lamb[30] lists five possible conduction

mechanisms through insulating thin films:

1. Schottky emission and the Poole-Frenkel effect
2. Tunneling and internal field emission
3. Space-charge-limited flow
4. Ionic conduction
5. Impurity conduction.

Schottky Emission and the Poole-Frenkel Effect

Schottky emission is a mechanism of current transport in which high-field emission of thermally activated electrons from a metal into the conduction band of an insulator in contact with the metal occurs.[31] Essentially, the applied field reduces the height of the metal-insulator interface barrier.[30] One characteristic of Schottky emission is its temperature dependence.

The Poole-Frenkel effect[30] is based on the same lowering of a barrier height by an applied electric field as the Schottky effect. In this case the barrier in question is that for thermal excitation of trapped electrons in the insulator into the conduction band of the insulator.

Tunneling and Internal Field Emission

For insulating films of 50 A or less, quantum mechanics studies have shown that electrons can pass from one electrode to the other by tunneling and internal field emission processes[1] that have been postulated to include:[30]

1. Electron transition from the valence to the conduction band - Zener breakdown.

2. Electron transition to the conduction band from localized impurity levels - field ionization.

3. Electron tunneling from the cathode in a similar manner to field emission into a vacuum.

4. Electron transition from the valence band to the anode.

Space-Charge-Limited Flow

The type of contact existing at the metal-insulator interface can be important in conduction processes in insulating thin films. Three types of contacts can exist:[1]

1. Ohmic contacts, where the electrode can readily supply electrons to the insulator as needed.

2. Neutral contacts, where no reservoir of charge exists at the contact.

3. Blocking contacts, where electrons can flow from the insulator into the metal to establish thermal equilibrium conditions.

Electrodes must be connected to the insulator to facilitate the injection of electrons into and their withdrawal from the bulk of the insulator. At moderate applied voltages, enough carriers will normally be available to enter the insulator from the negatively biased electrode to replenish the carriers leaving the bulk of the insulator at the other electrode. The bulk properties of the insulator determine the current-voltage characteristics of the sample; this type of conduction process is referred to as bulk-limited.[1] Higher electric fields or blocking contacts bring about emission-limited or contact-limited conduction. In this case, the current capable of being supplied by the

cathode (negatively biased electrode) to the insulator will be less than capable of being carried in the bulk of the insulator. Conditions existing at the cathode-insulator interface will primarily control the current-voltage characteristics of the sample.

Insulators too thick to allow tunneling and which do not contain donors will not normally conduct a significant current. If ohmic contact is made to the insulator, space-charge electrons can be injected into the conduction band of the insulator which are capable of carrying currents. This process is termed space-charge-limited conduction.[1] Charge unbalances can easily be produced by an applied voltage in insulators since insulators normally have a low density of free carriers and hence, space-charge-limited conduction can have a pronounced effect on the electrical properties of insulators at room temperature and below.[30]

Through the use of ohmic contacts, large amounts of space charge can be injected into the insulator. A large portion of the injected space charge will condense in traps contained in the insulator; occupancy of traps is a function of temperature[1] and thus space-charge-limited currents are temperature dependent. Increasing the applied voltage (injection level) will result in all traps eventually becoming filled and the current will rise to the trap-free value. Single carrier injected currents are necessarily space-charge-limited.[30]

Double injection,[30] where space-charge-limited currents of both types of carriers (holes and electrons) will flow in the insulator, occurs if the cathode is ohmic for electron flow and the anode is ohmic

for hole flow. Electrons will be injected from the cathode and holes from the anode. In this case, space-charge-limited conditions are at least partially overcome and for intermediate injection levels, charge neutrality can be assumed through the insulator. Space charge becomes important at high or low injection levels. Defect states, if present in the insulator, will have an influence on the current. Double injected currents will be larger than those due to single-carrier injection under the same conditions of voltage bias.

Current-voltage and current-temperature relationships for space-charge-limited conduction is presented in Table 2. Also included are the same relationships for tunnel emission and Schottky emission (after Emtage and Tantraporn[31]).

Ionic Conduction

Ionic conduction is due to the drift of defects under the influence of an applied electric field.[30] The actual mechanism of drifts is jumps of ions or vacancies over a potential barrier from one defect site to the next. Ionic conduction can also be due to moisture and consequently, those films which absorb moisture will have their ionic conduction enhanced.

Impurity Conduction

In an impure insulator, an electron occupying an isolated donor level has a wave function localized about the impurity and an energy slightly below the conduction band minimum. There is a small but finite overlap of the wave function of an electron of one donor with neighboring donors. Hence, a conduction process is possible in which

Table 2. Current-Voltage and Current-Temperature Relationships in Selected Conduction Mechanisms

Mechanism	Current-Voltage Dependence	Current Temperature Dependence
Space-Charge-Limited	$I \propto V^2$	$I \propto \mu$, the mobility of electrons in the insulator
Tunnel emission	$I \propto V$ for $V < \phi$ $I \propto V^2 \times e^{-\text{const}/V}$, for high V	None
Schottky emission	$I = \alpha \exp(\beta V^{1/2})$	$I \propto T^2 e^{-\text{const}/T}$

ϕ = working function between electron passing from metal to insulator

$\beta = (q^3/Ka)^{1/2}/kT$

q = charge on electron
a = thickness of insulator
K = relative dielectric constant of insulator

$\alpha = AT^2 e^{-\phi/kT}$

A = Richardson constant

the electron moves between centers without activation into the conduction band. This is known as impurity conduction.[30]

The presence of both donor and acceptor centers is a necessary condition for impurity conduction. Movement of electrons from an occupied donor to an unoccupied one is accomplished when acceptors remove a number of electrons from the donors. Impurity conduction is possible without acceptors only when a high concentration of impurities are present. For low impurity concentrations, electrons move by a hopping process from one center to another.

Electrical Properties of Thin Film and Bulk $Al_{2-x}Cr_xO_3$

Salama[32] studied conduction mechanisms in r.f. sputtered Al_2O_3 films utilizing Al-Al_2O_3-Si capacitive structures. Plotting current density versus the square root of the electric field resulted in two distinct regions. At high electric fields, the current varied exponentially with the square root of the electric field. At low electric fields, the characteristic was ohmic. Using gold electrodes rather than aluminum electrodes yielded similar results. It was suggested that the current was bulk-controlled rather than electrode-controlled because the conduction characteristics were found to be independent of film thickness (400-600 A), the electrode material, and the polarity of the electrodes. The current density, J_a, was based on three contributions (after Mead[33]), all bulk controlled,

$$J_a = J_{a1} + J_{a2} + J_{a3} \tag{3}$$

where

$$J_{a1} = C_1 E_a \exp(-q\phi_a/kT) \exp q/kT (\beta E_a)^{1/2} \quad (4)$$

$$J_{a2} = C_2 E_a^2 \exp(-E_2/E_a) \quad (5)$$

$$J_{a3} = C_3 E_a \exp(-q\phi_3/kT) \quad (6)$$

C_1, C_2, C_3, E_2, ϕ_3 = constants,

q = electronic charge,

ϕ_a = barrier height,

E_a = applied field,

k = Boltzman constant,

T = temperature in ^oK,

β = $a/\pi K_a \varepsilon_o$,

K_a = relative dielectric constant, and

ε_o = permittivity of free space.

Current density J_{a1} is due to field enhanced thermal excitation of trapped electrons into the conduction band (Poole-Frenkel effect) and occurs at high field gradients. Current density J_{a2} is due to field ionization of trapped electrons, a tunneling process independent of temperature which occurs at high field gradients. Current density J_{a3} is due to hopping of thermally excited electrons from one isolated state to another, occurring at low field gradients and resulting in ohmic characteristics.

Barbe and Herman[35] studied current transport mechanisms in reactively sputtered Cr_2O_3 films deposited on silicon substrates and test

glass pieces. The deposited films were then coated with 10,000 A of aluminum to use as a top electrode, which was biased positive with respect to the silicon substrate. The Cr_2O_3 films were approximately 1000 A thick. Between 21°C and 300°C, the current transport was found to be bulk controlled. Charge transport occurred by thermally activated hopping of carriers between localized states at electric fields less than 10^5 volts/cm described by the equation

$$(J)_{dc} \sim (V/d) \exp(-\phi_2/kT) \tag{7}$$

where

$(J)_{dc}$ = direct current density,

V = applied voltage,

d = dielectric thickness,

ϕ_2 = an activation energy,

T = temperature, and

k = Boltzman constant.

Above electric fields of 10^5 volts/cm, charge transport occurred due to electric field-assisted thermal ionization of donor-type centers (Poole-Frenkel effect).

Many investigations have studied the electrical properties of Al_2O_3 thin films. For Al-Al_2O_3-Al capacitor devices, with the Al_2O_3 film being r.f. sputtered, Pratt[26] found that with grounded electrodes the breakdown voltage was 5 to 70 volts with an average dielectric strength of 1.2×10^6 volts/cm. For floating electrodes, the breakdown voltage was 70 to 100 volts with an average dielectric strength of

5.26 x 10^6 volts/cm. In addition, with floating electrodes the resistivities of the Al_2O_3 film were greater than 10^{17} ohm-cm for film thickness of 2000 to 8000 A; dielectric strength was found to be thickness dependent, ranging from 8 to 2 x 10^6 volts/cm for the thickness range 900 to 8000 A. In another study of r.f. sputtered thin films of Al_2O_3, Pratt[16] found that the yield percentage, or percentage of nonshorted capacitors, was approximately 97 percent for electrode areas of 0.1935 cm^2 and approaching 100 percent for electrode areas of 0.0013 cm^2. For Al-Al_2O_3-Au capacitor devices with r.f. sputtered Al_2O_3 thin films, Mier and Buvinger[14] achieved resistivities between 10^{12} and 10^{15} ohm-cm. It was found that preheating the substrate prior to film deposition lessened the thermal shock during initial film growth, resulting in a better yield of good devices per slide. Salama[27] measured dielectric strengths between 2 and 8 x 10^6 volts/cm for Si-Al_2O_3-Al capacitor devices of r.f. sputtered Al_2O_3 films. Dielectric strengths greater than 6 x 10^6 volts/cm and resistivities greater than 5 x 10^{14} ohm-cm were reported by Tanaka and Iwauchi[28] for Si-Al_2O_3-Al and Si-Al_2O_3-Au capacitor devices of reactively sputtered Al_2O_3 films. Frieser,[15] in studying Si-Al_2O_3-Au capacitor devices of reactively sputtered Al_2O_3, found dielectric strengths of 4 x 10^5 volts/cm, increasing to 8 x 10^5 volts/cm on heating.

Ryabova and Savitskaya[29] obtained thin films of Al_2O_3-Cr_2O_3 mixtures by the decomposition of vapors in a current of oxygen of previously codeposited aluminum and chromium acetylacetonates with varying quantities of chromium acetylacetonate as follows: 1, 3, 10, 20, 30

and 40 percent. Films were obtained with resistivities from 10^7 to 10^{12} ohm-cm with decreasing Cr_2O_3 content. The resistivity of pure Al_2O_3 films was 10^{13} ohm-cm.

Due to its high resistivity, most measurements involving Al_2O_3 have been carried out at temperatures above 300°C. Results of conductivity measurements[20] showed the resistivity of bulk Al_2O_3 to vary from 10^{12} to 10^7 ohm-cm at 300°C. The differences have been attributed to the purity of the Al_2O_3, structure (polycrystalline or single crystal), atmosphere during the measurements, crystallographic direction, surface conduction and the type of metal-insulator contacts.

Studies of the conductivity of bulk Cr_2O_3 have been carried out at temperatures of 600°C and higher. Crawford and Vest[21] found the resistivity of single crystal, unoriented Cr_2O_3 to vary from 10^3 to $10^{2.7}$ ohm-cm at 700°C in varying O_2 pressures. Stone[22] measured the resistivity of Cr_2O_3 at 600°C as 10^2 ohm-cm in both oxygen and argon atmospheres.

Hensler and Henry[23] studied the electrical resistance of Al_2O_3-Cr_2O_3 mixtures in the temperature range 600°C to 1500°C. In general, the resistivity of Al_2O_3 decreased as the Cr_2O_3 content increased except at 1 mole percent Cr_2O_3 and 92 mole percent Cr_2O_3 where resistivity maxima were found. Samples containing up to 6 mole percent Cr_2O_3 had higher resistivities than pure Al_2O_3. It was postulated that for additions of Cr_2O_3 up to 6 mole percent in Al_2O_3 the more polarizable Cr^{3+} ion substituted for the smaller Al^{3+} ion and, after assuming a polar character, reduced the excess surface charge, thereby reducing

surface conduction. Further additions of Cr_2O_3 past 6 mole percent in Al_2O_3 imparts to the structure more of the electrical properties of Cr_2O_3.

A study by Vernetti and Cook[24] on the effect of metal oxide additions on the electrical conductivity of alumina produced results similar to those of Hensler and Henry.[23] One mole percent additions of Cr_2O_3 to a base body composed of 99 wt percent Al_2O_3 and 1 wt percent MgO resulted in a slight decrease in resistivity over that of the base body in the temperature range 600°C to 1000°C and an increase in resistivity above 1000°C. For a base body of 96 wt percent Al_2O_3, 1 wt percent CaO, 1 wt percent MgO and 2 wt percent SiO_2, additions of 1 mole percent Cr_2O_3 resulted in a reduction of resistivity in the temperature range 500°C to 1400°C. Additions of 4 mole percent Cr_2O_3 to the same base body resulted in a decrease in resistivity of over two orders of magnitude up to 1100°C.

Measurements by Eremenko and Beinish[25] also found the resistivity of Al_2O_3-Cr_2O_3 mixtures to decrease from 100 mole percent Al_2O_3 to 100 mole percent Cr_2O_3 in the temperature range 100°C to 900°C. It was concluded that a continuous variation in the composition of the solid phase in the Al_2O_3-Cr_2O_3 system corresponded to a continuous variation in the electrical conductivity.

Physical Properties of Bulk and Thin Film $Al_{2-x}Cr_xO_3$

Wyckoff[9] states that in oxide systems where small metal ions allow cation radius to anion radius ratios of less than 0.60, the oxygen atoms can approach nearer to a perfect close-packing. Such an

arrangement results in metallic sesquioxides with rhombohedral symmetry with each unit cell containing two molecules. The space group is $D_3d^6(R\bar{3}c)$ and the atoms are in the following special positions:

R(metal) - uuu; $\bar{u}\bar{u}\bar{u}$

X(Oxygen) - $v\bar{v}o$; $\bar{v}ov$; $ov\bar{v}$; 1/2 - v, v + 1/2, 1/2; v + 1/2, 1/2, 1/2 - v; 1/2, 1/2 - v, v + 1/2.

where u, v = constant parameters which determine atom positions in the unit cell. Both α-Al_2O_3 and Cr_2O_3 are included in this group of sesquioxides. Such an arrangement as described above can best be illustrated as a slightly distorted hexagonal close packing of oxygen ions with small metal ions lying in some of the interstices.

In his studies of the Al_2O_3 and Cr_2O_3 structures, Davey[10] describes each unit prism as containing three molecules, resulting in the structure of a diamond except for a stretching of the body-diagonal. High axial ratios found in these systems can be explained by assuming a hexahedral molecule consisting of an equilateral triangle of oxygen with a metal atom immediately above and below the center of the triangle.

Alumina, Al_2O_3, can occur in at least seven forms,[11] with the two most common forms being "gamma" alumina (cubic) and "alpha" alumina (hexagonal). Transformation of "gamma" alumina to the more stable "alpha" alumina occurs in the temperature range of 750°C to 1200°C. Chromia, Cr_2O_3, occurs only in the hexagonal form. Table 3 lists some of the properties of Al_2O_3 and Cr_2O_3.

If incorporation of foreign atoms into a host structure leads to a large lowering of the free energy of the system, a new crystalline

Table 3. Selected Properties of Al_2O_3 and Cr_2O_3[11]

Material	Crystal System	Theoretical Density (g/cm^3)	Melting Point (^oC)
α-Al_2O_3	Hexagonal	3.98 $\pm$ 0.02	2049 $\pm$ 5
γ-Al_2O_3	Cubic	3.65	- -
Cr_2O_3	Hexagonal	5.21	2299 $\pm$ 104

form will develop.[12] Solid solutions are stable when the solution crystal has a lower free energy than the alternatives--building up two crystals of different composition or building up a new structure in which foreign atoms are put on ordered sites. Studies have indicated that the system α-Al_2O_3 - Cr_2O_3 forms a continuous series of solid solutions.[13] X-ray spectrograms of α-Al_2O_3 - Cr_2O_3 demonstrate that no compounds are formed, but that complete miscibility occurs in the solid state. Solid solution in this system is substitutional,[12] where substitution of one ion for another occurs.

Mier and Buvinger[14] found the composition of r.f. sputtered alumina films to more nearly approximate α-Al_2O_3 although none of the films were exactly α-Al_2O_3. Electron diffraction studies showed the films to be a mixture of α and γ phases of Al_2O_3. These films were deposited at a maximum temperature of 300°C. Frieser[15] discovered two types of reactively sputtered alumina films: (1) a polycrystalline γ-Al_2O_3 film at high deposition rates and substrate temperatures, and (2) an amorphous Al_2O_3 film at low deposition rates and substrate temperatures. Temperatures during deposition of the Al_2O_3 films varied from 100°C to 600°C. The structure of Al_2O_3 films r.f. sputtered onto borax coated glass by Pratt[16] indicated uniform, fine textured amorphous films. Electron diffraction and dark field studies did not show the presence of any crystalline structure for films deposited at substrate temperatures up to 500°C. Salama[17] found r.f. sputtered Al_2O_3 films to be amorphous when examined by low-angle electron diffraction.

The densities[15] of either amorphous or gamma alumina thin films

obtained through reactive sputtering were found to be 1.8 ± 0.2 g/cm^3, about one-half that of bulk γ-Al_2O_3, which is 3.43 to 3.67 g/cm^3. Studies of the density of r.f. sputtered Al_2O_3 films as a function of power density[17] showed that low power depositions resulted in lower film densities. Density ranged from 3.5 g/cm^3 at a power density of 1 W/cm^2 to 3.8 g/cm^3 at a power density of 2.5 W/cm^2. Thus, a wide range of Al_2O_3 thin film densities have been obtained depending on deposition parameters.

Pratt[16] found r.f. sputtered Al_2O_3 films to show good affinity for aluminum with the deposited film possessing a high degree of smoothness. On evaporated copper and gold, adherence of Al_2O_3 varied from fair to poor.

Relatively little information on Cr_2O_3 thin films is available in the literature. Barbe and Herman[35] deposited Cr_2O_3 films through reactive sputtering of chromium in an argon-oxygen atmosphere. The films had the characteristic green color of Cr_2O_3 and were found to be amorphous.

CHAPTER III

PROCEDURE

Electrical properties of $Al_{2-x}Cr_xO_3$ thin films were investigated. The experimental procedure was divided into three distinct areas: fabrication of the sputtering targets, deposition of the thin films, and measurement of electrical properties. A separate discussion on each of these areas is presented in this Chapter. Other procedures such as the determination of the composition of each target and thin film, although mentioned briefly here, are discussed more thoroughly in the Appendices.

Fabrication of the R.F. Sputtering Targets

Two sets of targets were prepared. The first set consisted of nine compositions ranging in composition from 100 mole percent Al_2O_3 to 100 mole percent Cr_2O_3, Table 4. The Al_2O_3 was calcined alumina XA-15 (high purity) from Alcoa Chemicals and the Cr_2O_3 was Fisher certified chromium sesquioxide (99.7 percent pure) from Fisher Scientific Company. These weighed-out mixtures of oxides were wet-mixed in a blender under the conditions listed in Table 5. Drying of the oxide mixtures was accomplished in several days, with subsequent screening of the mixture (excluding 100 mole percent Al_2O_3 and 100 mole percent Cr_2O_3) through a 60-mesh screen. Air drying of the oxide mixtures was necessary since the binder (Polytran FS) used separates from the mixture at the elevated temperatures existing in a gas dryer. Pressing

Table 4. Target Compositions - Set I

Mole Percent Cr_2O_3	Moles Cr_2O_3	Moles Al_2O_3	Wt. Al_2O_3 (g)	Wt. Cr_2O_3 (g)	Total Wt. (g)
0	0	3.923	400 ± 0.1	0	400 ± 0.1
12.5	0.461	3.237	330 ± 0.1	70 ± 0.1	400 ± 0.2
25.0	0.875	2.619	267 ± 0.1	133 ± 0.1	400 ± 0.2
37.5	1.244	2.069	211 ± 0.1	189 ± 0.1	400 ± 0.2
49.9	1.572	1.579	161 ± 0.1	239 ± 0.1	400 ± 0.2
62.4	1.875	1.128	115 ± 0.1	285 ± 0.1	400 ± 0.2
75.0	2.151	0.716	73 ± 0.1	327 ± 0.1	400 ± 0.2
87.5	2.401	0.343	35 ± 0.1	365 ± 0.1	400 ± 0.2
100.0	3.632	0	0	400 ± 0.1	400 ± 0.1

Table 5. Mixing Conditions for Set I Targets

Mole Percent Cr_2O_3	Composition Wt. (g)	H_2O Content (ml)	Binder Wt. (g)	Mixing Time (min)
0	400 ± 0.1	-	-	-
12.5	400 ± 0.2	500 ± 10	20 ± 0.1	3
25.0	400 ± 0.2	500 ± 10	20 ± 0.1	3
37.5	400 ± 0.2	500 ± 10	20 ± 0.1	3
49.9	400 ± 0.2	500 ± 10	20 ± 0.1	3
62.4	400 ± 0.2	600 ± 10	20 ± 0.1	3
75.0	400 ± 0.2	600 ± 10	20 ± 0.1	3
87.5	400 ± 0.2	600 ± 10	20 ± 0.1	3
100.0	400 ± 0.1	-	-	-

of the samples into disk targets involving mixing the oxide mixture with a small percentage of water, screening through a 20-mesh screen, and pressing in a Denison hydraulic press to 3-1/2 inch diameter at pressures of 6000-8000 psi. After a 16-hour drying period, the disks were fired in a Harrop globar furnace over a two-day span, with the maximum temperature reaching 1480°C. Upon cooling, the disks were transferred to a gas-air kiln, fired slowly up to a maximum temperature of 1705°C where they were held for several hours. The globar furnace was used initially because its firing schedule can be precisely controlled, resulting in more uniform firing of the samples.

The second set of targets consisted of 4, 8, 16 and 20 mole percent Cr_2O_3 in Al_2O_3, Table 6. These oxide mixtures were wet-mixed in a blender for 3-minute intervals with 300 ml additions of water and no binder, and dried in a gas dryer for 16 hours. After screening through a 60-mesh screen to obtain a powder, disks were prepared by mixing the powder with small percentages of water, passing through a 35-mesh screen, and uniaxially pressing in a small hydraulic hand press to 2-1/4 inch diameter disks at 10,000 psi. Firing of the disks was accomplished using a gas-air furnace at a maximum temperature of 1705°C.

Thin Film Preparation

Capacitive devices were produced with $Al_{2-x}Cr_xO_3$ insulating films sandwiched between aluminum electrodes. A schematic of capacitive device fabrication is shown in Figure 2. First, a glass substrate was coated with aluminum, the dielectric film was sputtered leaving an exposed aluminum edge for electrical contact, and then 0.079 cm^2 aluminum

Table 6. Target Compositions - Set II

Mole Percent Cr_2O_3	Moles Cr_2O_3	Moles Al_2O_3	Wt. Al_2O_3 (g)	Wt. Cr_2O_3 (g)	Total Wt. (g)
4	0.042	1.00	101.96 ± 0.1	6.38 ± 0.1	108.34 ± 0.2
8	0.087	1.00	101.96 ± 0.1	13.22 ± 0.1	115.18 ± 0.2
16	0.190	1.00	101.96 ± 0.1	28.88 ± 0.1	130.84 ± 0.2
20	0.250	1.00	101.96 ± 0.1	38.00 ± 0.1	139.96 ± 0.2

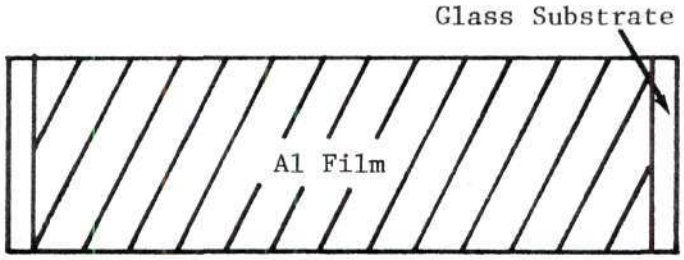

(a). Bottom Electrode Deposition.

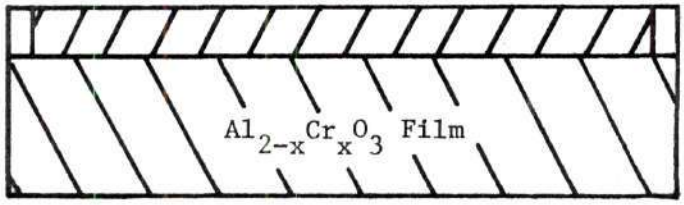

(b). Sputtered Film Deposition.

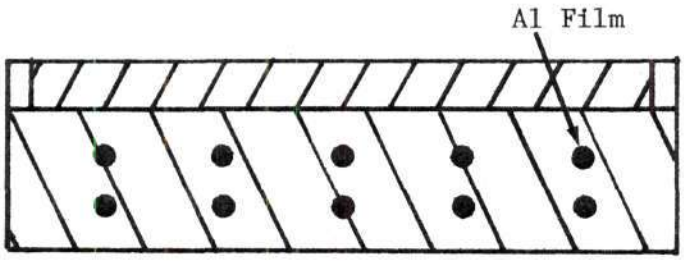

(c). Top Electrode Deposition.

Figure 2. Schematic of Capacitive Device Fabrication.

electrodes were deposited over the dielectric.

Thin film preparation was divided into three areas:

1. Substrate cleaning,
2. Electrode deposition, and
3. Thin film sputtering.

Substrate Cleaning

Soda-lime glass microscope slides, 1 inch by 3 inches, were selected as the substrates. The following method was used to clean every substrate:

1. Ultrasonic cleaning of the slides in a borax soap solution for 15 minutes.
2. Repeated rinses in distilled water.
3. Ultrasonic cleaning in aqua regia (1 part concentrated HNO_3, 3 parts concentrated HCl, 4 parts water) for 15 minutes.
4. Repeated rinses in distilled water.
5. A rinse in acetone, followed by a rinse in methanol.

After cleaning, the substrates were stored in a covered container to minimize dust contamination.

Electrode Deposition

Aluminum (99.999 percent pure) was used as the electrode material because thin films of Al_2O_3 adhere well to it, it is easily vacuum evaporated, and it adheres well to the substrate. The aluminum electrodes were evaporated at pressures lower than 10^{-5} torr to thicknesses between 800 A and 1200 A as monitored with a piezoelectric microbalance. The bottom electrode was deposited on the substrate over an area approximately 17.00 cm^2 while the ten top electrodes, 0.3175 cm

in diameter, were applied through a metal mask. Typical aluminum electrode depositions lasted for about five minutes.

Sputtering of $Al_{2-x}Cr_xO_3$ Thin Films

All dielectric films were deposited using a R. D. Mathis SP310 r.f. sputtering system operating at 13.56 MHz. During the sputtering process, the following parameters were recorded at selected time intervals--p.a. grid, plate current, pressure, reflected power, r.f. voltage, dc voltage, and temperature. Temperature readings approximating that of the substrate were made possible using a type S thermocouple positioned at the bottom electrode in the work chamber of the sputtering unit.

The sputtering targets were attached to the top electrode using Torr Seal, a low pressure resin. The work chamber was always evacuated to a pressure of 2×10^{-6} torr or lower before gas was admitted. Gas used to sustain the glow discharge in all cases was high purity, 9.89 percent oxygen in argon. Pressure in the work chamber was maintained at $5.5 - 6.5 \times 10^{-3}$ torr after initiation of the glow discharge by use of a leak valve and the position of the gate valve to the diffusion pump. Initiation of the glow discharge was accomplished by increasing the p.a. grid to between 80 and 100 ma, adjusting the r.f. voltage to between 3 and 4 kv, and then, after switching to the dc voltage reading, increasing the pressure in the work chamber until the glow discharge started. After initiation of the glow discharge, the reflected power was adjusted to its minimum value to ensure the most efficient sputtering from the target. A shutter, separating the glow discharge from the

substrate, was kept closed for five minutes after the start of the glow discharge to clean the target surface. All dielectric deposition times were for 60 minutes, except in two cases where 90-minute deposition times were used. A typical set of data collected for a deposition is illustrated in Table 7. During each deposition, adjustments in the settings had to be made continuously to minimize parameter variations.

Electrical Measurements

Resistances in ohms for the thin films were obtained directly using a Keithley 610C solid state electrometer. Contact was made by the use of small wires which had been silver pasted to the bottom and top electrodes of each capacitive device. A time interval of 5 to 10 minutes was usually needed for the resistance measurement to stabilize. From the resistance of the thin film, resistivity could be calculated using Equation 1.

Breakdown voltages for each film were obtained using the circuit shown in Figure 3. A Keithley 610C solid state electrometer was used to monitor current and a Hewlett-Packard 419A dc null voltmeter was used to monitor voltage. The voltage was supplied by an Electronic Research Associates, Inc. tubeless power supply model 110DMC. Contacts were made in the same manner as in resistance measurements. As the voltage across the film was increased slowly, two voltage values were recorded--the voltage at which the first sign of film breakdown was detected and the voltage at which massive film breakdown occurred (defined in this case to be when the surrounding film not covered by the electrode was destroyed). It must be stressed that these values

Table 7. Typical Set of Data Collected During $Al_{2-x}Cr_xO_3$ Film Deposition

Time (min)	P.A. Grid (ma)	Plate Current (ma)	Pressure (torr)	Reflected Power	R.F. Voltage (kv)	DC Voltage (kv)	Temperature (°C)
2	80	340	$6x10^{-3}$	1.00	3.30	2.40	345
15	80	340	$6x10^{-3}$	1.20	3.40	2.45	435
30	80	340	$6x10^{-3}$	1.20	3.50	2.45	420
45	80	340	$6x10^{-3}$	1.25	3.50	2.40	420
57	80	340	$6x10^{-3}$	1.25	3.55	2.45	425
60 Experiment terminated							

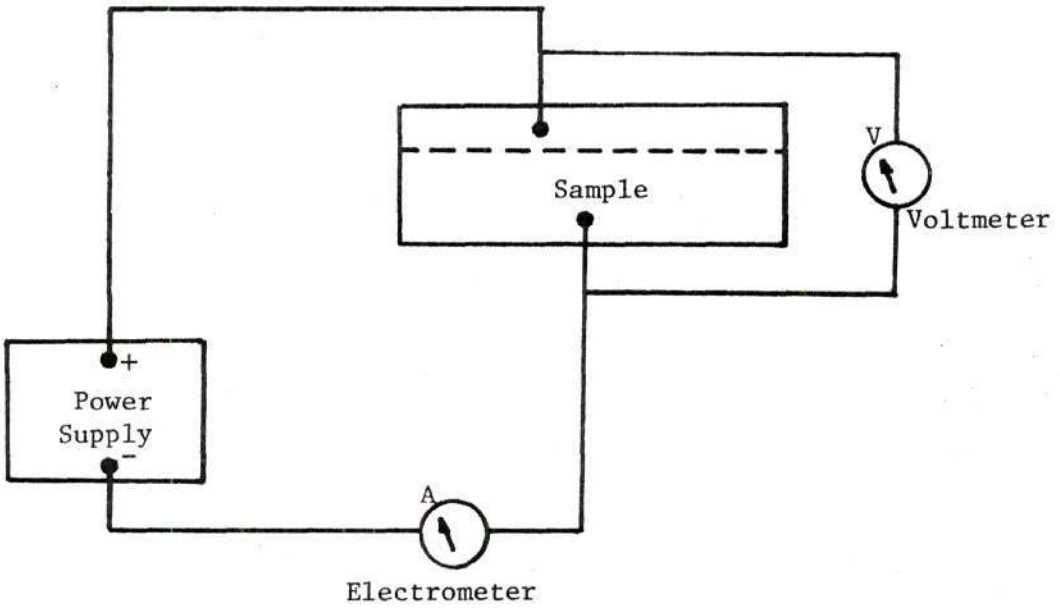

Figure 3. Circuit Used to Obtain Breakdown Voltages.

were used as boundary values and that breakdown of the film occurred continuously within these limits. Dielectric strength could be obtained from the breakdown voltages using Equation 2.

Current-voltage measurements were made using a Keithley 610C solid state electrometer to monitor current and a Hewlett-Packard model 721A power supply. The power supply was equipped with two scales--0 to 10 volts and 0 to 30 volts--and since voltages of greater than 6 to 8 volts were capable of causing film breakdown, a 10:1 voltage divider was incorporated into the circuit, Figure 4, to control voltage between 0 and 3 volts with greater accuracy. At low voltages, the current was typically in the range 10^{-10} to 10^{-11} amperes. At low currents, the measurements were unstable and had to be taken inside an aluminum box to shield the sample from stray electrical signals. Measurements were also made with and without a grounded shield around the top electrode, with no differences in the measurements being detected. The grounded shield, Figure 5, was used as a deterrent to leakage currents reaching the top electrode from the bottom electrode. In many cases, 5 to 10 minutes were needed for the current measurements to stabilize sufficiently to be recorded, especially in the low current ranges.

Physical and Chemical Property Determination

To determine if the fired targets had assumed a complete solid solution, X-ray diffraction patterns were obtained from powder samples of each fired target composition (see Appendix A). The actual composition of each target after firing was determined using X-ray fluorescence techniques (see Appendix A). Densities of the targets were

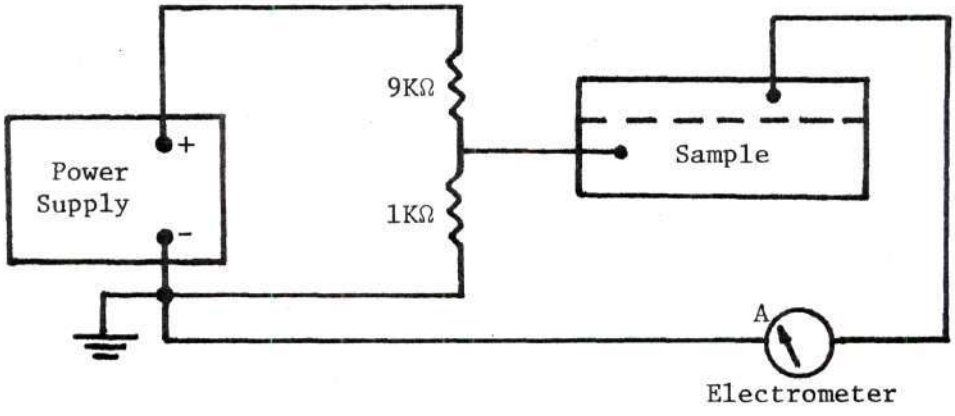

Figure 4. Circuit Used in Current-Voltage Measurements.

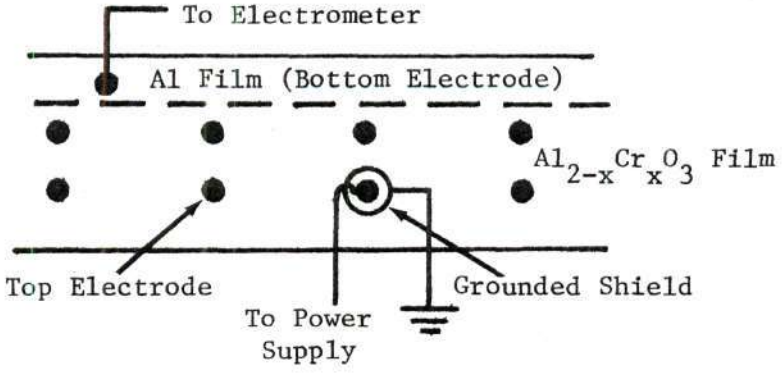

Figure 5. Configuration Used in Shielding Top Electrode from Leakage Currents.

estimated from the data obtained by Thilo et al.[34] in their studies of the Al_2O_3-Cr_2O_3 system, Figure 6.

Physical and chemical properties of the thin $Al_{2-x}Cr_xO_3$ films were not as easily obtained. Since more sophisticated methods and techniques of exact determination were not available, the composition of each film was assumed to be that of the target. Relative chromium contents of the films were measured using a scanning electron microscope equipped with a nondispersive X-ray energy analyzer. Nondispersive X-ray traces were generated by 20 kev electrons and the resulting X-rays were collected for time intervals of 400 seconds. The area under the chromium peak in each case was divided by the thickness of the film to normalize the chromium intensities because the film thickness was small compared to the penetration depth.

As was the case with composition, the density of each $Al_{2-x}Cr_xO_3$ film was assumed to be the same as that of the target, although the actual density of the film could be much lower. Film thickness was determined through weight changes in the substrate before and after deposition, knowing that the volume of the film times its density equals its weight change. Although this method of film thickness determination is the least accurate, it has the advantage in that average film thickness over the entire deposition area is provided. Electron diffraction techniques were used to determine if the films were amorphous or crystalline.

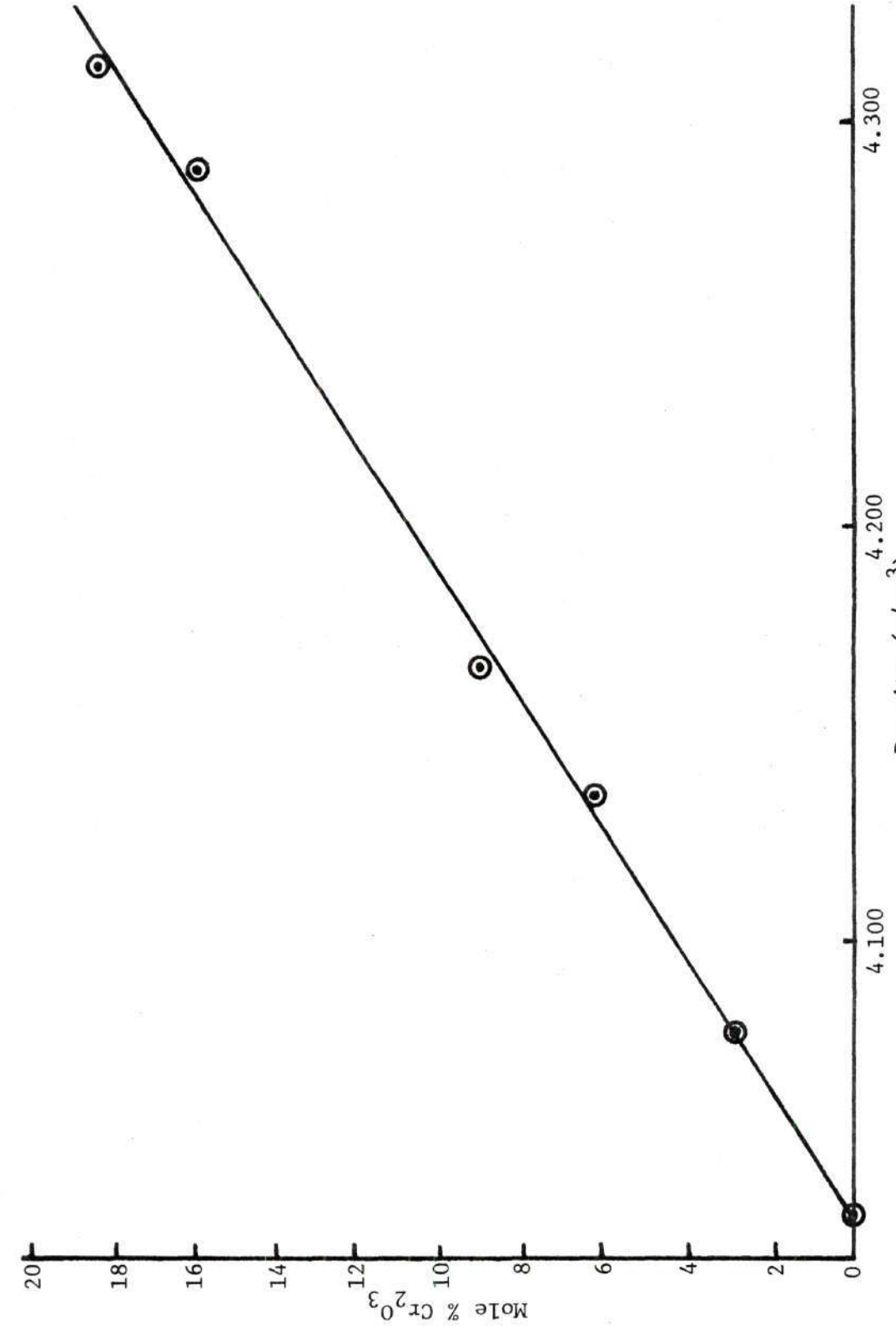

Figure 6. Mole Percent Cr_2O_3 in Al_2O_3 As a Function of Density.[34]

CHAPTER IV

RESULTS AND DISCUSSION

The first section of this Chapter discusses the results of the physical and chemical studies on the sputtering targets and the $Al_{2-x}Cr_xO_3$ thin films. The subsequent sections focus on the results of the electrical measurements. Separate discussions are presented on current-voltage measurements and possible conduction mechanisms, resistivity measurements, and dielectric strength measurements.

Target and Film Properties

Examination of the first set of targets showed all those compositions above 25 mole percent Cr_2O_3 to be poorly sintered; subsequent sputtering trials with several of the targets from this set--25.0, 37.5 and 75.0 mole percent Cr_2O_3--resulted in cracking of the targets due to thermal gradients established in the target during the sputtering process. Two targets from this set, 100 mole percent Al_2O_3 and 12.5 mole percent Cr_2O_3, performed successfully and were utilized in the deposition work. All of the targets in the second set were well sintered and did not crack. Hence, all of the targets from Set II were used in the investigation. The dimensions of the six targets used, along with their fired composition as determined from X-ray fluorescence (see Appendix A) are listed in Table 8. Color of the targets varied from light pink at 4.1 mole percent Cr_2O_3 to grayish pink at 19.0 mole percent Cr_2O_3.

Table 8. Target Compositions and Dimensions

Composition			
Unfired	Fired	Target Diameter (cm)	Target Thickness (cm)
0	0	8.10 ± 0.02	0.45 ± 0.02
4.0	4.1*	5.00 ± 0.02	0.55 ± 0.02
8.0	7.8	5.10 ± 0.02	0.62 ± 0.02
12.5	11.8	7.90 ± 0.02	0.60 ± 0.02
16.0	14.6	5.25 ± 0.02	0.55 ± 0.02
20.0	19.0	5.30 ± 0.02	0.57 ± 0.02

*Although this composition should not be greater than the unfired composition, it is within the experimental error of the technique used to determine fired compositions and hence will be used as the fired composition.

Physical appearance of the sputtered films for the most part was the same. All of the films were transparent, varying in color from light pink and yellow on the same sample to blue, purple, red, and yellow on a single sample; the majority of the samples exhibited a color of light pink or red to yellow. The lighter pink film color was typical of the target colors for the lower mole percent Cr_2O_3 compositions. On several samples, the Al film after sputtering possessed a yellowish-gold tint. This was attributed to trapped impurities or diffusion pump oil in the Al film during the evaporation process which reacted with the oxygen in the sputtering gas during the film deposition.

An examination of the $Al_{2-x}Cr_xO_3$ films under transmitted light in the microscope indicated many small inhomogeneities existing in the Al film (bottom electrode) since light was transmitted through them (a slide coated with Al only showed no transmitted light.) These inhomogeneities increased in size with increasing temperature as indicated by various portions of the Al film, Figure 7. Temperature gradients at the substrate surface were due to proximity to the glow discharge. Region T_1 (Figure 7) was protected by a metal mask and temperature increased with distance away from the mask. The inhomogeneities are larger in the sputtered portion, which was subjected to higher temperatures. In some samples, those portions of the Al film reaching the highest temperatures (almost directly under the center of the sputtering target) showed dendritic growth. In these areas, the Al film seemed to be almost completely destroyed. Maximum temperatures reached in any of the film depositions were approximately $450^{o}C$. Apparently, these

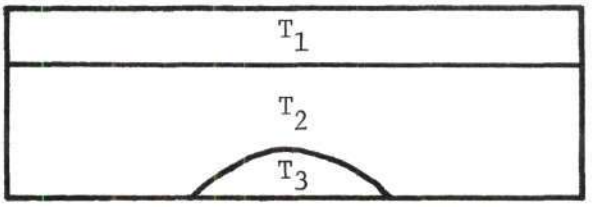

(a) Physical Setup ($T_1 < T_2 < T_3$).

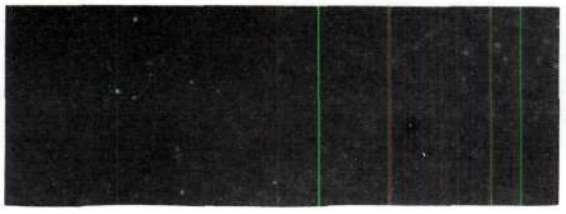

(b) Region T_1

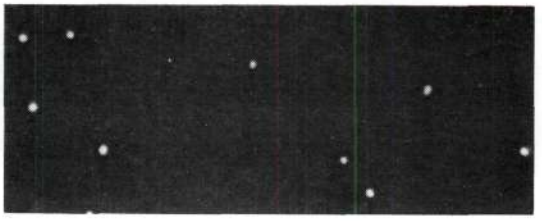

(c) Region T_2 (near T_1).

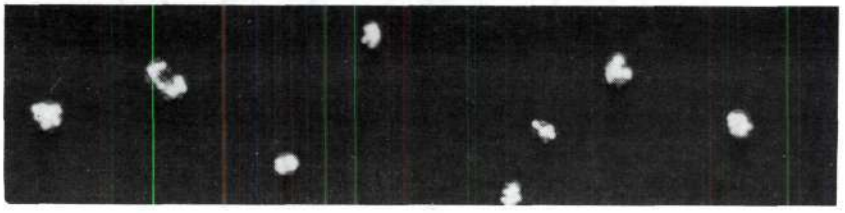

(d) Region T_2 (near T_3).

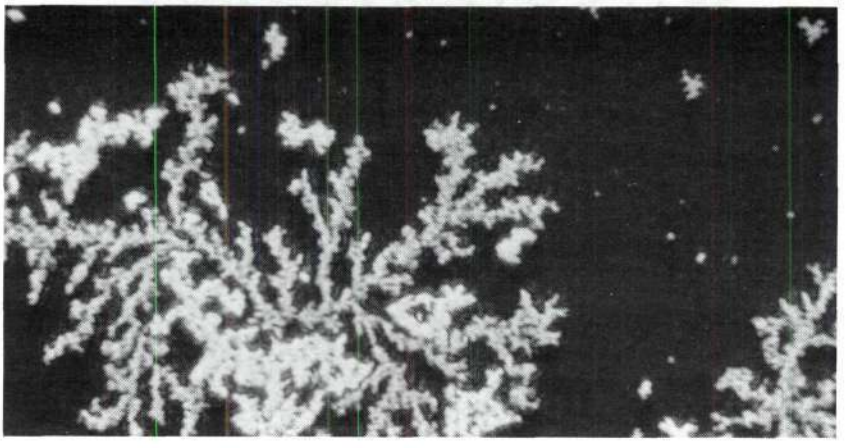

(e) Region T_3 Showing Dendritic Growth.

Figure 7. Varying of Al Film Oxidation with Temperature. Transmitted Light, X750.

inhomogeneities are the initiation of dendritic growth, caused by the Al film reacting with the oxygen in the sputtering gas to form Al_2O_3.

Electron diffraction patterns were obtained for all but the 100 mole percent Al_2O_3 film, Figure 8. The films were all polycrystalline, although the degree of crystallinity varied. Diffraction patterns of the 7.8, 11.8 and 19.0 mole percent Cr_2O_3 films were fairly sharp, indicating better crystallinity and larger crystallite size than in the 4.1 and 14.6 mole percent Cr_2O_3 films, which had very fuzzy diffraction patterns. The crystal structure for the 7.8, 11.8 and 19.0 mole percent Cr_2O_3 films was the same as γ-Al_2O_3, but the accuracy of the lattice parameter measurements was insufficient to provide composition information. The diffuse nature of the 4.1 and 14.6 mole percent Cr_2O_3 patterns indicated that these films lacked long-range order but possessed some short-range order.

The compositions of the sputtered films were assumed to be that of the targets. Nondispersive X-ray traces of the films showed the chromium peak in increasing mole percent Cr_2O_3 films to be increasing in height and area, Figure 9, thus indicating increasing chromium content in the films. Dividing the area under each peak by the film thickness (to normalize reulsts) and plotting versus mole percent Cr_2O_3 showed this increase to be essentially linear, Figure 10, indicating that the thin film chromium content was in the ratio of the target chromium contents.

Physical characteristics of the sputtered films along with deposition rates during sputtering are listed in Table 9. The density of

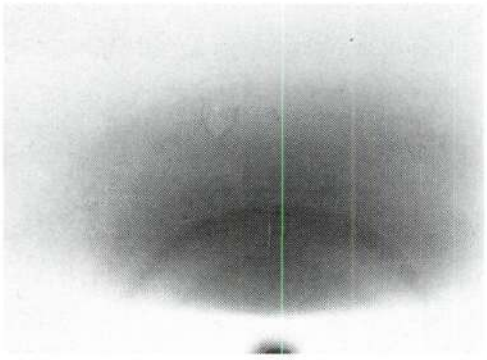

(a). 4.1 Mole Percent Cr_2O_3.

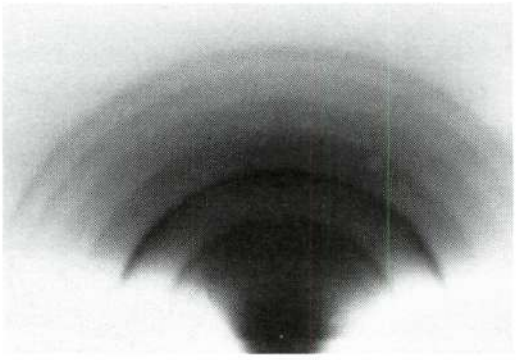

(b). 7.8 Mole Percent Cr_2O_3.

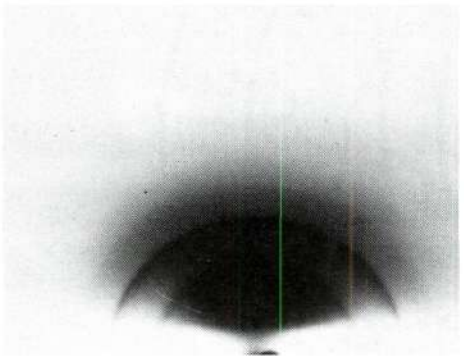

(c). 11.8 Mole Percent Cr_2O_3.

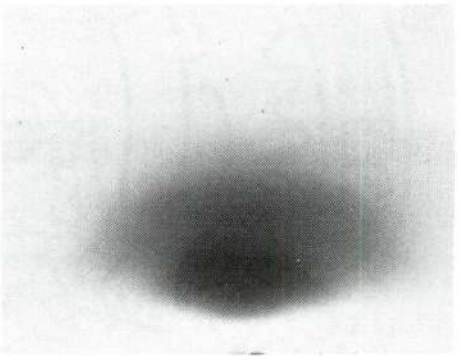

(d). 14.6 Mole Percent Cr_2O_3.

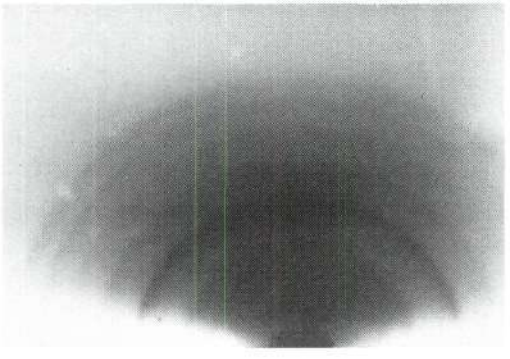

(e). 19.0 Mole Percent Cr_2O_3.

Figure 8. Electron Diffraction Patterns for the $Al_{2-x}Cr_xO_3$ Films.

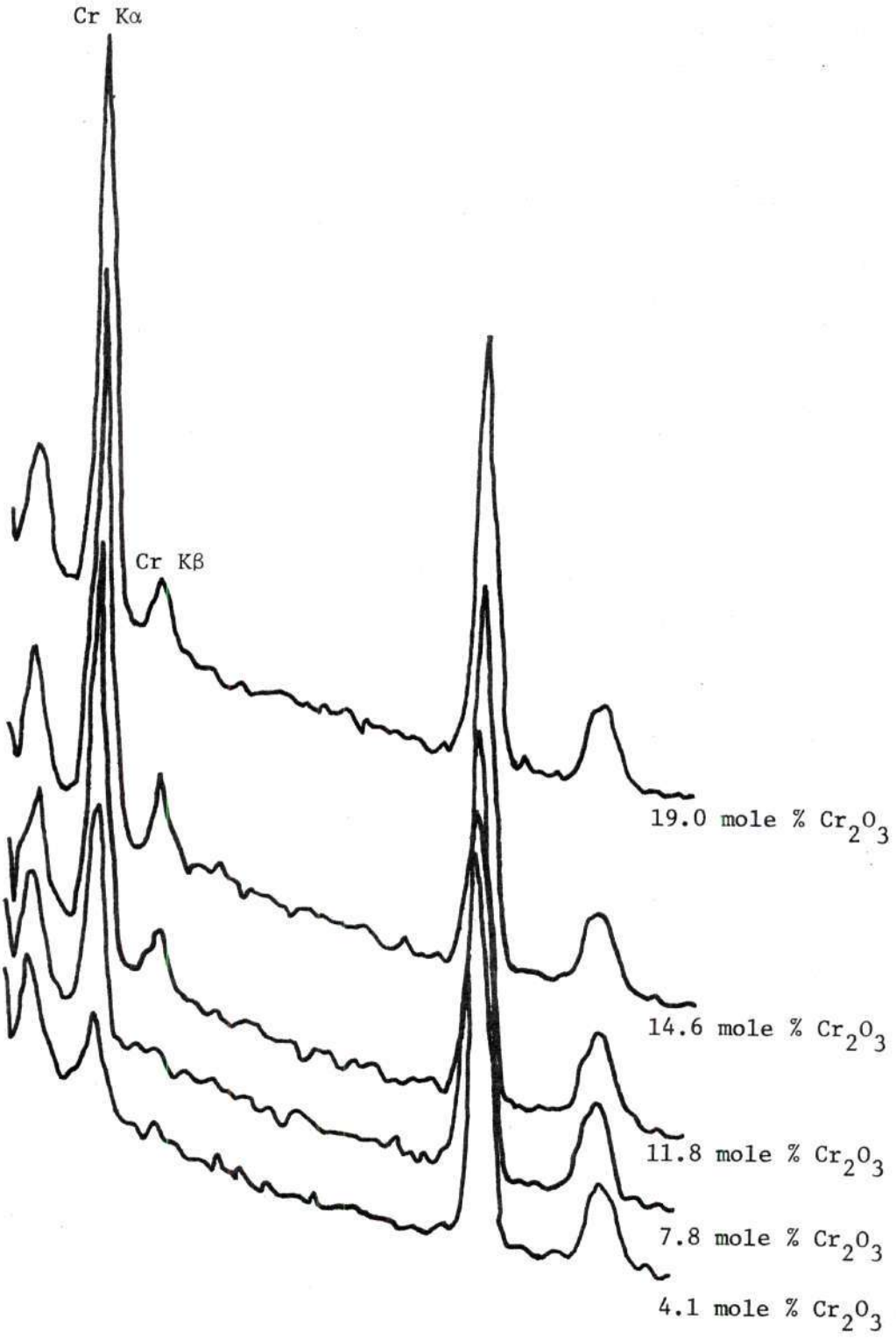

Figure 9. Nondispersive X-ray Traces of $Al_{2-x}Cr_xO_3$ Thin Films Increasing in Chromium Content.

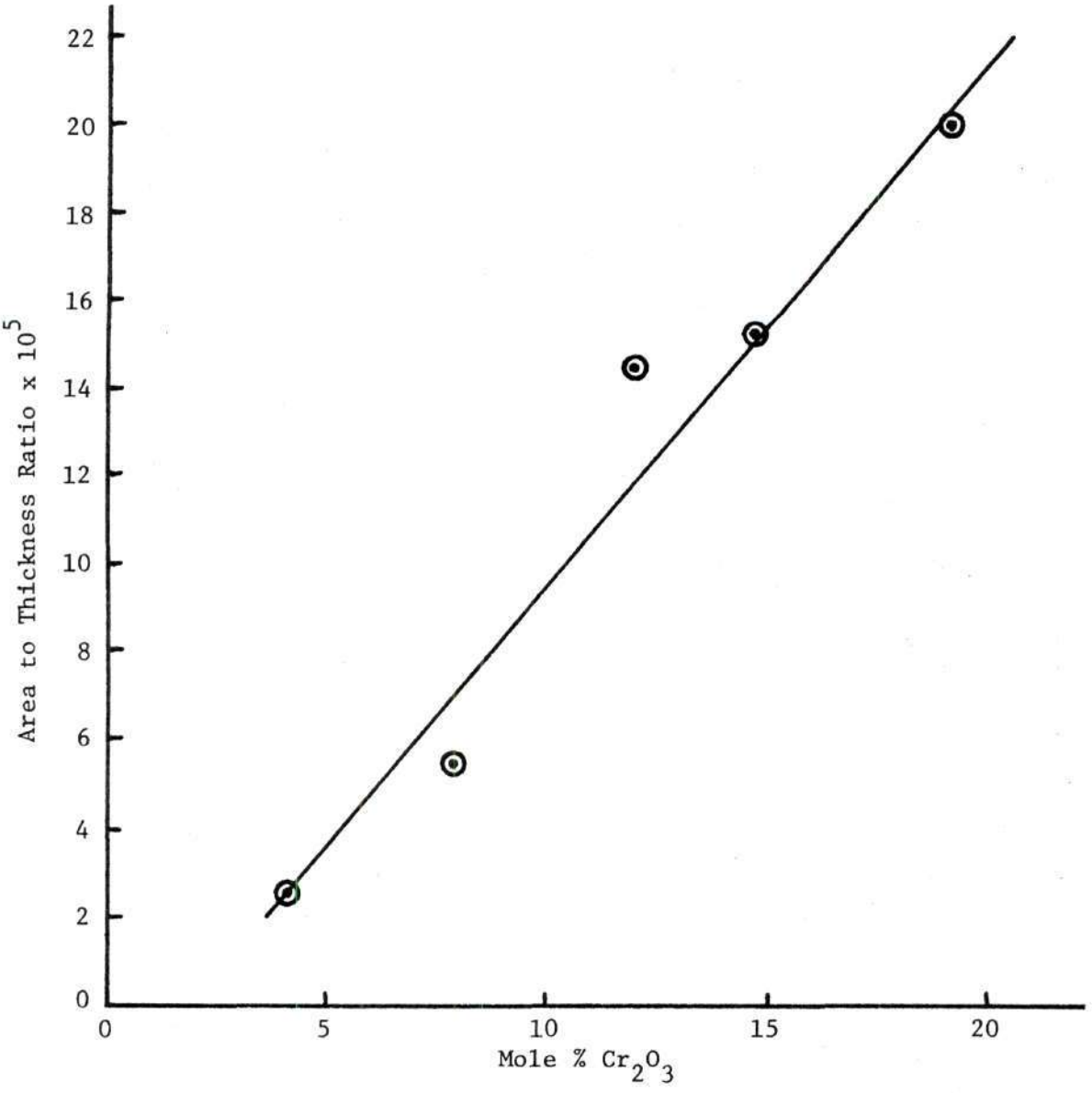

Figure 10. Normalized Cr Kα Peak Area As a Function of Mole Percent Cr_2O_3 in Al_2O_3.

Table 9. Physical Characteristics of the Sputtered Films

Composition (mole % Cr_2O_3)	Sample No.	Film Density (g/cm^3)	Film Area (cm^2)	Film Weight (g)	Film Thickness (A)	Deposition Rate (A/min)
0	40-43.1	4.032	12.19	0.0007	1420	23.7
	40-43.2	4.032	12.19	0.0006	1220	20.3
4.1	40-59.1	4.096	13.72	0.0009	1600	26.7
	40-59.2	4.096	13.72	0.0011	1950	32.5
	40-60.1	4.096	13.72	0.0010	1770	29.5
	40-60.2	4.096	13.34	0.0010	1830	30.5
	40-61.1	4.096	14.10	0.0012	2070	34.5
	40-61.2	4.096	13.72	0.0012	2130	35.5
7.8	40-53.1	4.154	12.95	0.0009	1670	27.8
	40-53.2	4.154	13.34	0.0012	2160	36.0
	40-54.1	4.154	13.34	0.0012	2160	36.0
	40-54.2	4.154	12.19	0.0011	2170	36.2
	40-55.1	4.154	12.57	0.0010	1910	31.8
	40-55.2	4.154	12.95	0.0010	1850	30.8
11.8	40-45.1	4.216	12.57	0.0008	1500	25.0
	40-45.2	4.216	12.57	0.0008	1500	25.0
	40-46.1	4.216	11.43	0.0011	2280	38.0
	40-46.2	4.216	12.19	0.0013	2520	42.0
	40-47.1	4.216	12.57	0.0008	1500	25.0
	40-47.2	4.216	12.19	0.0009	1750	29.2

Table 9. Physical Characteristics of the Sputtered Films (Contd.)

Composition (mole % Cr_2O_3)	Sample No.	Film Density (g/cm^3)	Film Area (cm^2)	Film Weight (g)	Film Thickness (A)	Deposition Rate (A/min)
11.8	40-49.1	4.216	12.95	0.0008	1460	24.3
	40-49.2	4.216	12.95	0.0008	1460	24.3
14.6	40-56.1	4.260	14.10	0.0011	1830	30.5
	40-56.2	4.260	13.34	0.0011	1930	32.2
	40-57.1	4.260	13.72	0.0010	1710	28.5
	40-57.2	4.260	13.72	0.0011	1880	31.3
	40-58.1	4.260	12.95	0.0008	1450	24.2
	40-58.2	4.260	13.72	0.0009	1530	25.5
19.0	40-50.1	4.328	12.95	0.0010	1780	19.8
	40-50.2	4.328	13.34	0.0011	1900	21.1
	40-51.1	4.328	13.34	0.0007	1210	13.4
	40-51.2	4.328	12.95	0.0007	1240	13.8
	40-52.1	4.328	11.43	0.0007	1410	23.5
	40-52.2	4.328	11.81	0.0007	1360	22.7

the film was assumed to be that of the target, although studies have shown that the density can be as much as 50 percent lower.[15] The method used to calculate thickness resulted in an average minimum film thickness since theoretical density based on the hexagonal solid solution structure was used. It is highly probable that film thickness is not uniform throughout the film. Deposition rates varied as was expected since target dimensions as well as the recorded parameters during film deposition varied, although every effort was made to keep the parameters within reasonable limits for successive depositions.

Current-Voltage Relationships

Conduction mechanisms were studied for the 4.1, 7.8, 14.6 and 19.0 mole percent Cr_2O_3 films. Current measurements were recorded from 0.3 volt to 3.0 volts in increments of 0.3 volt. Conversion to current densities and the square root of the applied electric field, $\sqrt{E}$, (see Appendix D) were used to normalize results. The average results for each composition are listed in Table 10, and plotted in Figures 11 - 14. Clearly visible slope changes in the 4.1 and 19.0 mole percent Cr_2O_3 curves indicate that more than one conduction mechanism was present in those films. No such slope changes were evident in the 7.8 and 14.6 mole percent Cr_2O_3 films. However, if the actual film thickness varied considerably from the calculated thickness, then the curves could be shifted into an electric field range in which only one conduction mechanism exists since the current would pass more easily through the thinnest portion of the film.

Salama,[32] in plotting J versus $\sqrt{E}$ for r.f. sputtered Al_2O_3 films,

Table 10. Average $\sqrt{E}$ and J Values for the Sputtered Films

Composition (mole % Cr_2O_3)	$\sqrt{E} \times 10^{-2}$ ($[V/cm]^{1/2}$)	$J \times 10^{9}$ (A/cm^2)	Composition (mole % Cr_2O_3)	$\sqrt{E} \times 10^{-2}$ ($[V/cm]^{1/2}$)	$J \times 10^{9}$ (A/cm^2)
4.1	1.26	0.146	14.6	1.32	0.064
	1.78	0.260		1.87	0.151
	2.19	0.390		2.30	0.382
	2.53	0.686		2.65	0.940
	2.82	1.31		2.96	2.02
	3.10	3.82		3.24	4.02
	3.34	16.1		3.50	7.30
	3.57	52.6		3.75	12.7
	3.79	100.0		3.98	20.6
	4.00	144.0		4.19	36.0
7.8	1.24	0.175	19.0	1.44	0.348
	1.75	0.686		2.04	0.822
	2.14	1.46		2.49	1.64
	2.48	4.57		2.88	2.74
	2.77	8.90		3.22	7.42
	3.03	17.4		3.52	12.7
	3.28	31.3		3.80	25.0
	3.50	51.0		4.06	54.8
	3.72	77.9		4.32	97.7
	3.92	324.0		4.46	162.0

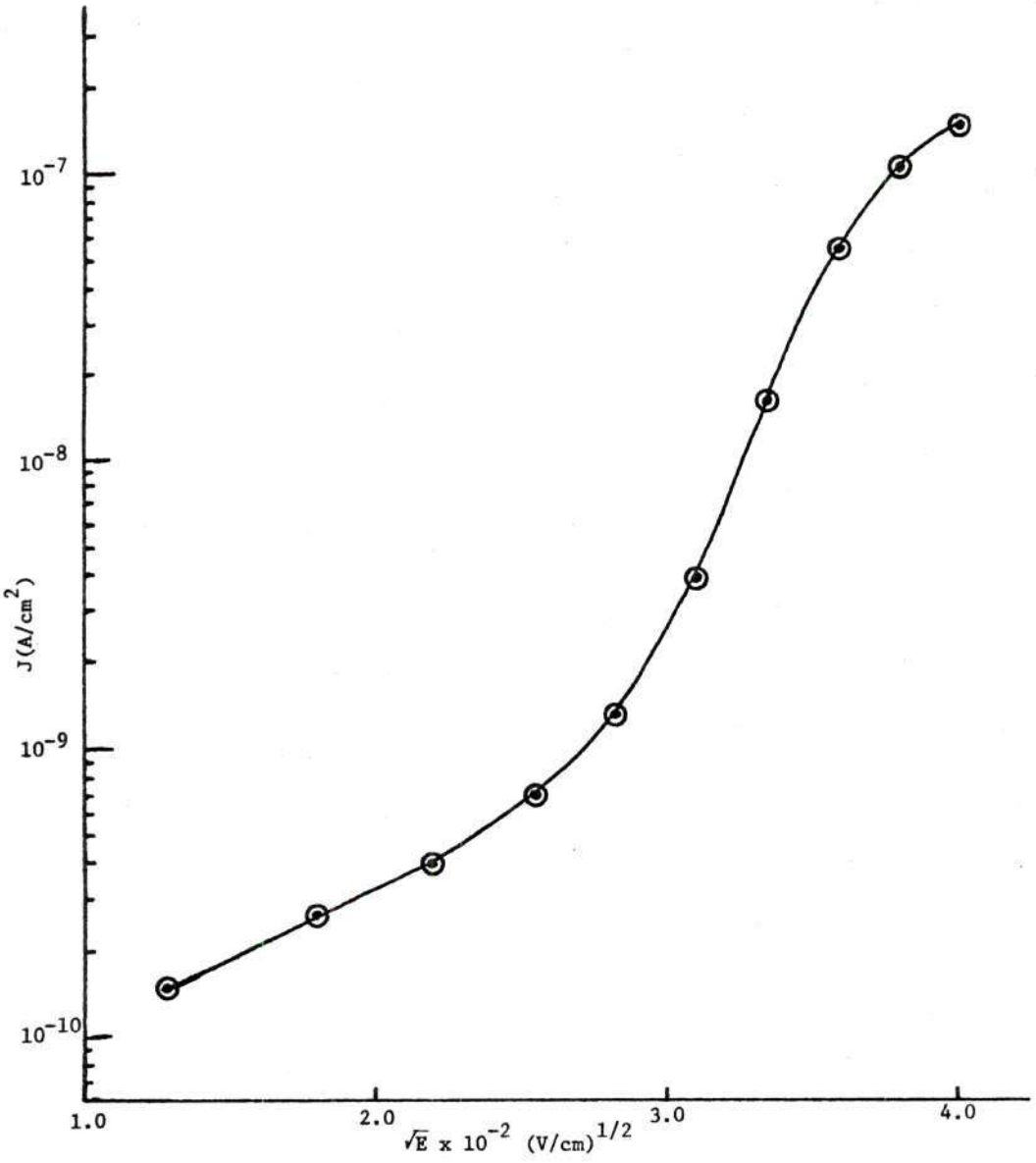

Figure 11. Current Density As a Function of the Square Root of the Applied Electric Field for 4.1 Mole Percent Cr_2O_3 in Al_2O_3.

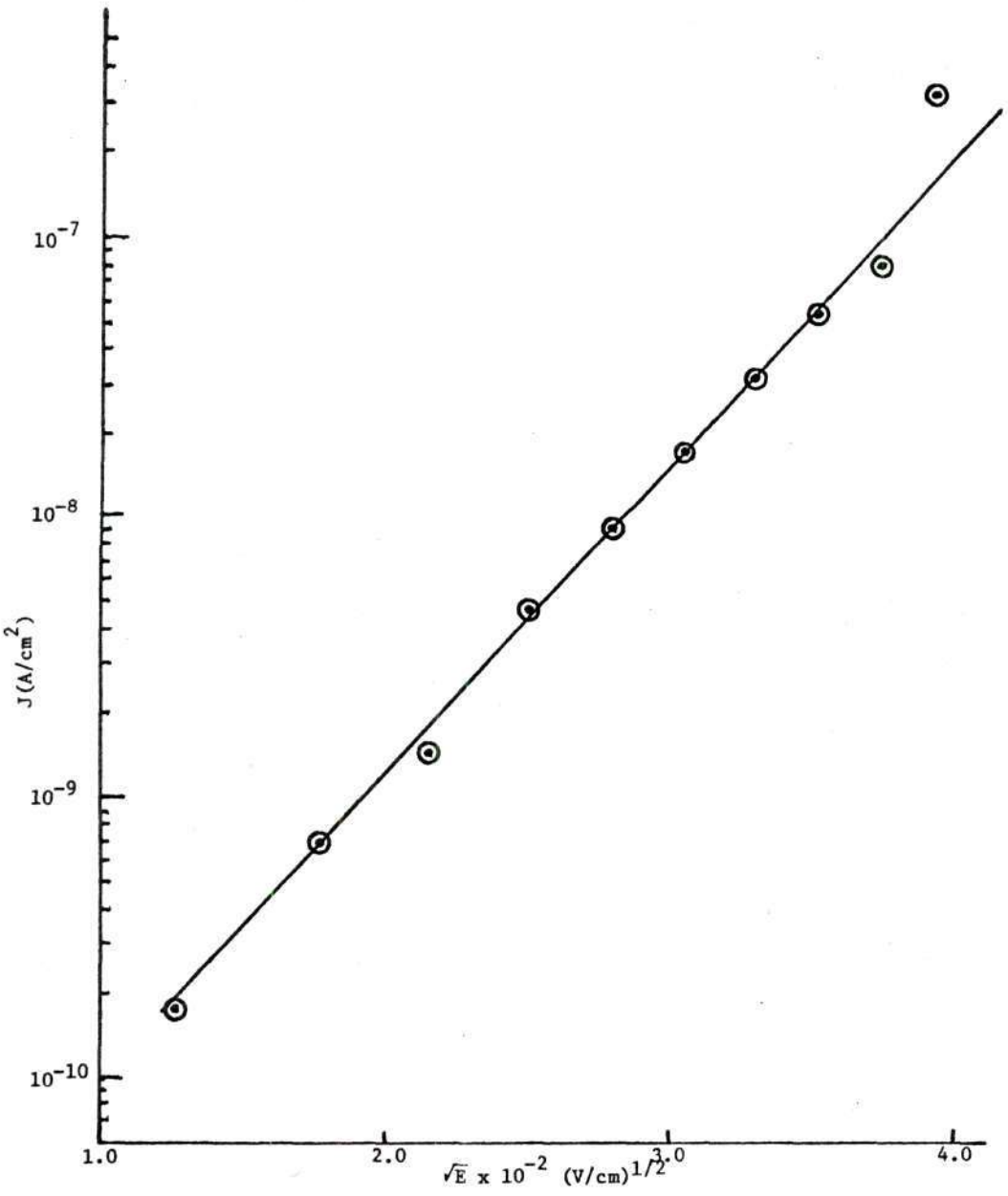

Figure 12. Current Density As a Function of the Square Root of the Applied Electric Field for 7.8 Mole Percent Cr_2O_3 in Al_2O_3.

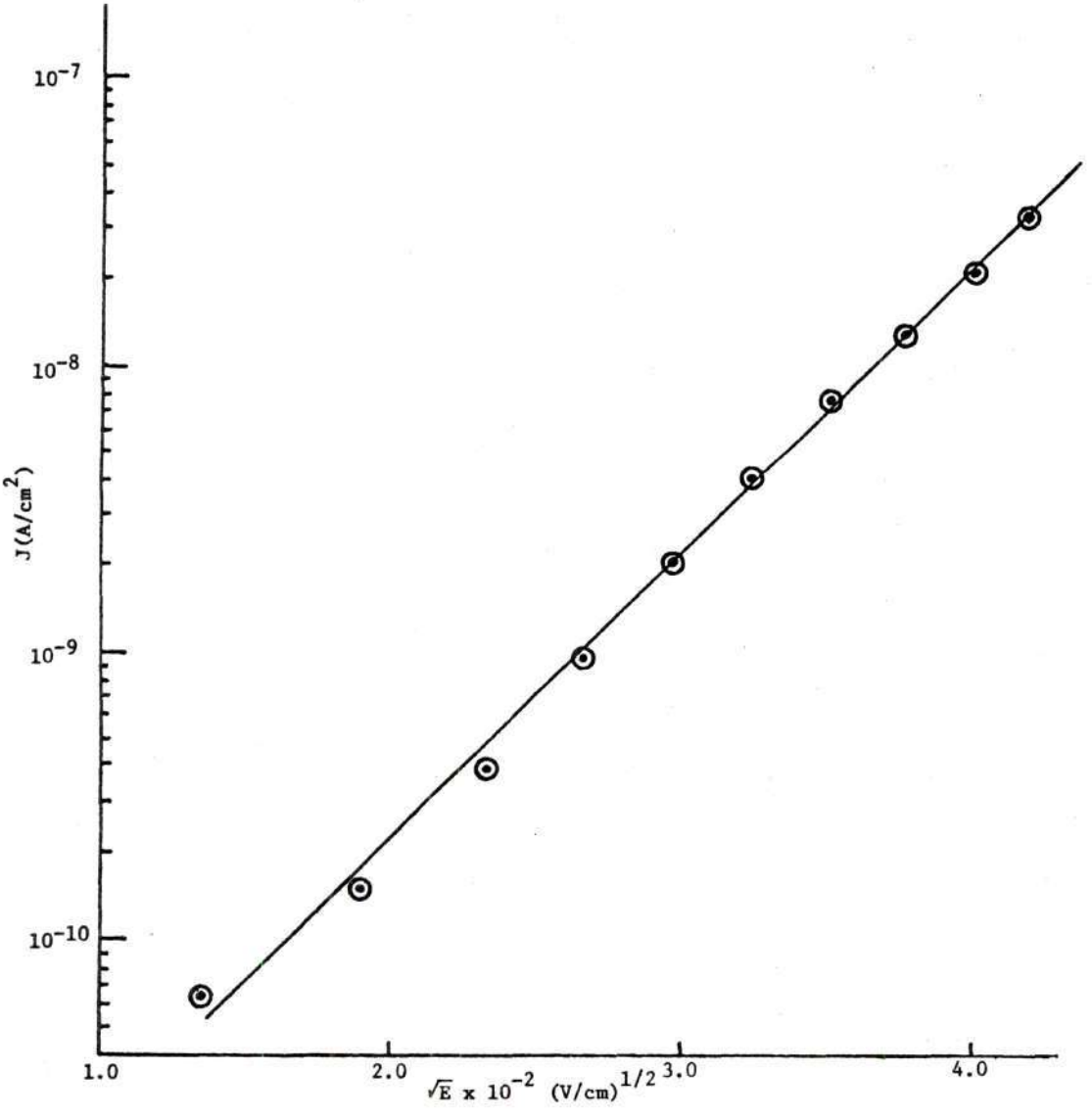

Figure 13. Current Density As a Function of the Square Root of the Applied Electric Field for 14.6 Mole Percent Cr_2O_3 in Al_2O_3.

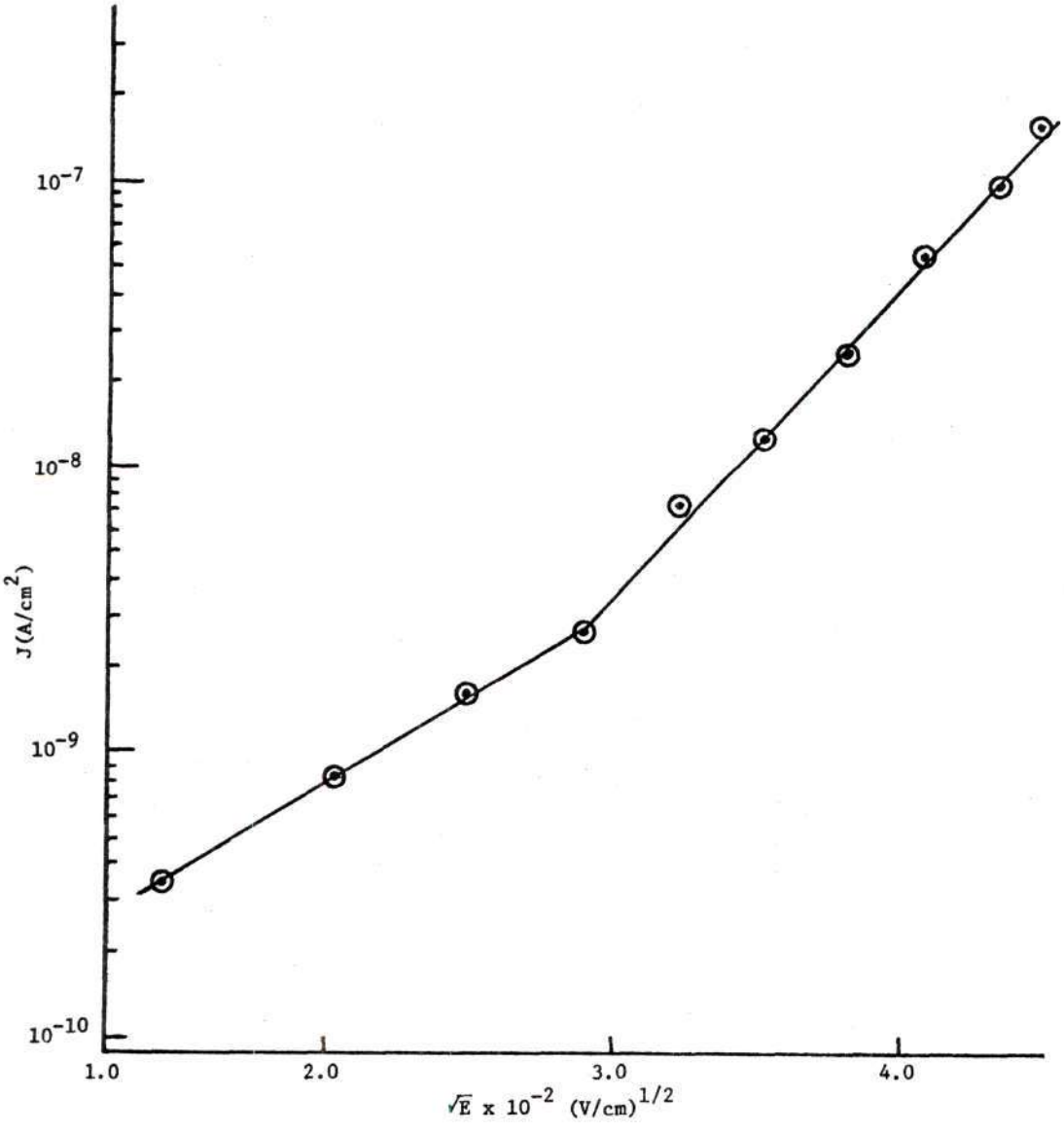

Figure 14. Current Density As a Function of the Square Root of the Applied Electric Field for 19.0 Mole Percent Cr_2O_3 in Al_2O_3.

had results similar to those observed for the 4.1 mole percent Cr_2O_3 film. At low field gradients below the change in slope, he determined that conduction exhibiting ohmic characteristics was the main mode of conduction and above this change the Poole-Frenkel conduction mechanism predominated. In those results, however, no relaxation in slope of the curve was present as in the 4.1 mole percent Cr_2O_3 sample at the higher electric fields. The lower portion of the 4.1 mole percent Cr_2O_3 curve does approximate ohmic conduction since voltage varies directly with current (R = constant). The portion above the break appeared to vary exponentially with $\sqrt{E}$, characteristic of the Poole-Frenkel type conduction. Further studies on temperature dependence need to be investigated to verify this since the current density varies exponentially with a term involving temperature. No explanation could be offered for the relaxation in slope of the upper portion of the curve. Salama also found the ohmic - Poole-Frenkel transition to occur at higher electric fields than in the 4.1 mole percent Cr_2O_3 case. The Cr_2O_3 content may shift this transition to lower applied fields.

Barbe and Herman[35] studied J versus $\sqrt{V}$ (square root of the applied voltage) in reactively sputtered Cr_2O_3 thin films, and attained curves similar to the curve for the 19.0 mole percent Cr_2O_3 film, Figure 14. Their change in slope occurred at approximately 2.0×10^5 volts/cm, whereas on the 19.0 mole percent Cr_2O_3 curve it occurred at approximately 9.0×10^4 volts/cm. In the upper voltage range, Barbe and Herman found Poole-Frenkel conduction which was verified by temperature dependence studies and at the lower voltage range thermally activated

hopping of carriers between localized states (ohmic conduction) was verified by frequency dependence studies. Consequently, although two types of conduction mechanism definitely appear to exist in the 19.0 mole percent Cr_2O_3 film, frequency and temperature dependence studies are needed to positively identify them as the conduction mechanisms which Barbe and Herman found to exist. Since Salama[32] and Barbe and Herman[35] had reported the same conduction mechanisms for Al_2O_3 and Cr_2O_3, respectively, it was not surprising to find evidence for these same mechanisms in the $Al_{2-x}Cr_xO_3$ films.

Only one type of conduction mechanism appeared to exist in the 7.8 and 14.6 mole percent Cr_2O_3 films. The slopes in these two curves were almost identical to that of the upper slope in the 19.0 mole percent Cr_2O_3 curve. Thus, the same type of conduction mechanism should exist in these films as in the region with the same slope in the 19.0 mole percent Cr_2O_3 curve, most likely Poole-Frenkel type conduction. The appearance of only one type of conduction mechanism could possibly be due to a thickness variation in the film shifting the field gradient to higher ranges.

Space-charge-limited conduction did not exist in any of the films studied. According to Emtage and Tantraporn,[31] I is proportional to V^2 in SCL conduction and I versus V^2 calculations for the films showed this not to exist. Tunneling as one of the conduction mechanisms cannot exist because the films are too thick; tunneling can only occur in films less than or equal to 50 A in thickness. Schottky emission is similar to Poole-Frenkel type conduction and it is a possible conduction

mechanism in the films. As in Poole-Frenkel type conduction, Schottky emission is temperature dependent and such studies need to be made to determine if Schottky emission is one of the conduction mechanisms.

Resistivity

Resistivities of all the sputtered films (see Appendix B) were calculated using a resistance obtained by a constant current method; in such a method, voltage across the sample could not be arbitrarily set, but it was limited to a range of 0 to 1 volt. Since theoretical density was used as the density of the films, the thickness calculated is the minimum thickness that could exist in the film if the film is uniform. Thus, all resistivities calculated are close to the maximum resistivities associated with the sputtered film, with error introduced because of the almost certain nonuniformity of thickness associated with each film.

Resistivity ranges as well as average values are plotted in Figure 15 for the various mole percent Cr_2O_3 samples. A range of several orders of magnitude was expected and would be in the range of experimental error. Normal variations in the thicknesses of the films would be enough to explain the resistivity ranges observed in the 0 and 4.1 mole percent Cr_2O_3 samples. Statistical bar graphs were prepared for each of the remaining compositions in an effort to explain the large resistivity ranges, Figure 16. These graphs indicated that in the 7.8, 14.6 and 19.0 mole percent Cr_2O_3 samples very few resistivities are below 10^{13} ohm-cm. The graph for 11.8 mole percent Cr_2O_3 indicates that the average resistivity is high when compared with the number of

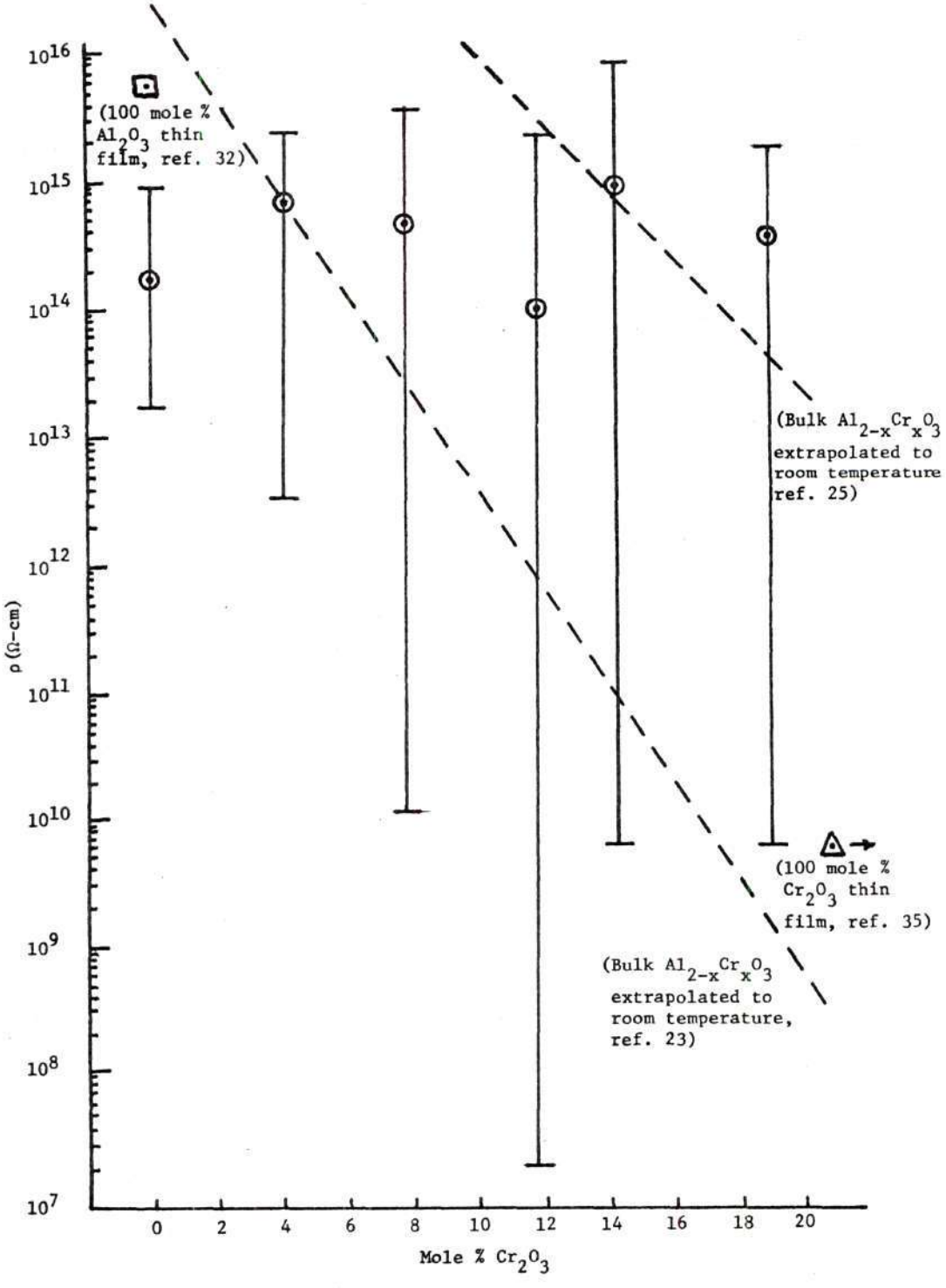

Figure 15. Resistivity Ranges with Average Resistivity Values for the $Al_{2-x}Cr_xO_3$ Films.

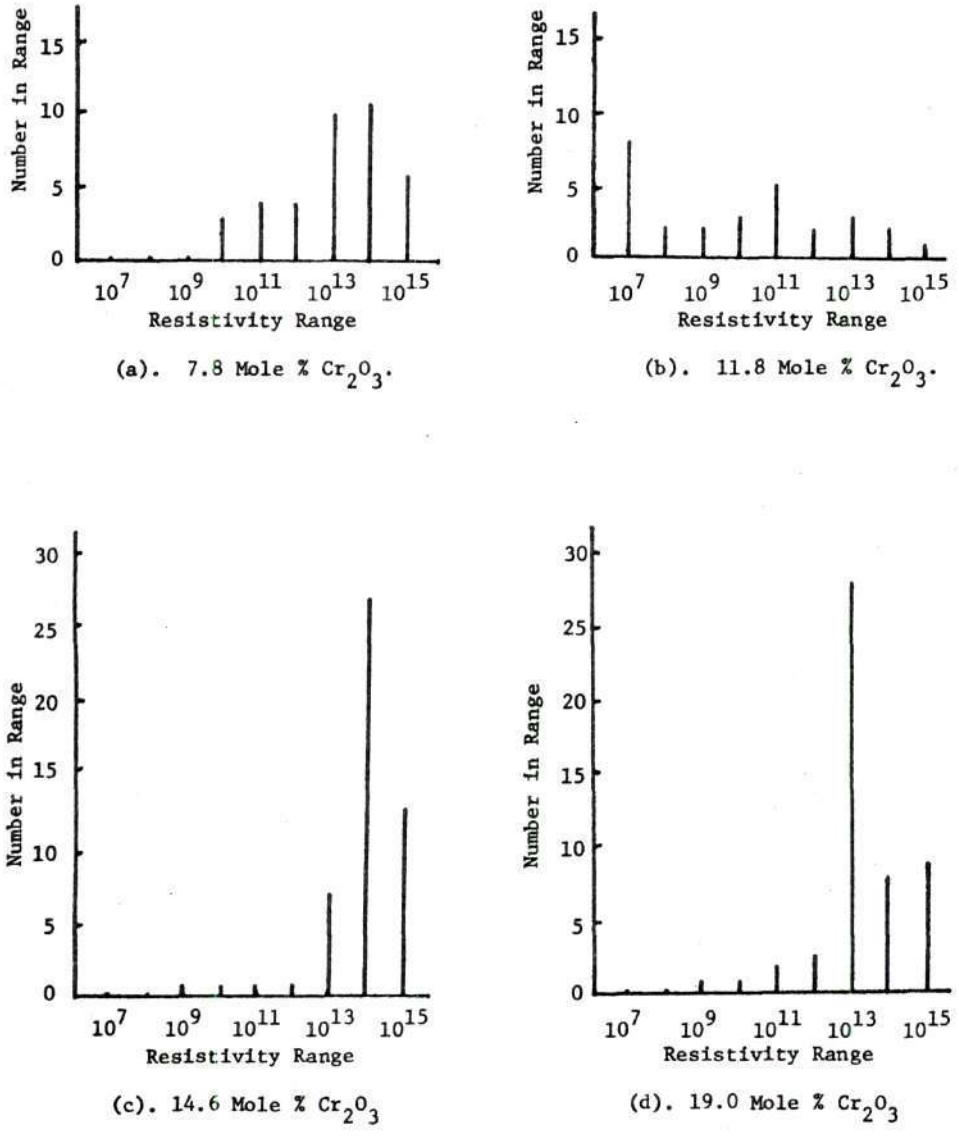

Figure 16. Statistical Bar Graph Showing Resistivity Spread.

resistivities in the 10^{12} to 10^{15} ohm-cm range. A study of yield percent of good capacitive devices per composition was as follows: 0 mole percent Cr_2O_3--85 percent; 4.1 mole percent Cr_2O_3--87 percent; 7.8 mole percent Cr_2O_3--63 percent; 11.8 mole percent Cr_2O_3--58 percent; 14.6 mole percent Cr_2O_3--85 percent; and 19.0 mole percent Cr_2O_3--87 percent. A large number of defects such as pinholes or breaks in the 7.9 and 11.8 mole percent Cr_2O_3 samples caused shorting. Pinholes or breaks which did not propagate through the entire thickness of the film could have caused thin spots in the films, resulting in resistivity measurements which were too low. Thus, thickness differences caused by defects could result in a wide range of resistivity values.

Oxidation of the aluminum bottom electrode did not measurably affect resistance measurements. It would be expected to affect resistivity measurements because resistivity varies directly with electrode area. Any oxidation of the Al film lowers the electrode area capable of conducting current, with a subsequent lowering of calculated resistivities. This varying electrode area was small and subsequent error in the resistivity of the film would be small.

The current density-applied electric field relationships showed the resistance to change with voltage except in the ohmic region of the 4.1 mole percent Cr_2O_3 film. The applied voltage can and does vary in a constant current method of measuring resistance. To establish the significance of this voltage change on resistivity, resistivity as a function of Cr_2O_3 content at selected voltages has been plotted in Figure 17. Within a voltage range of 2.7 volts, the resistivities of

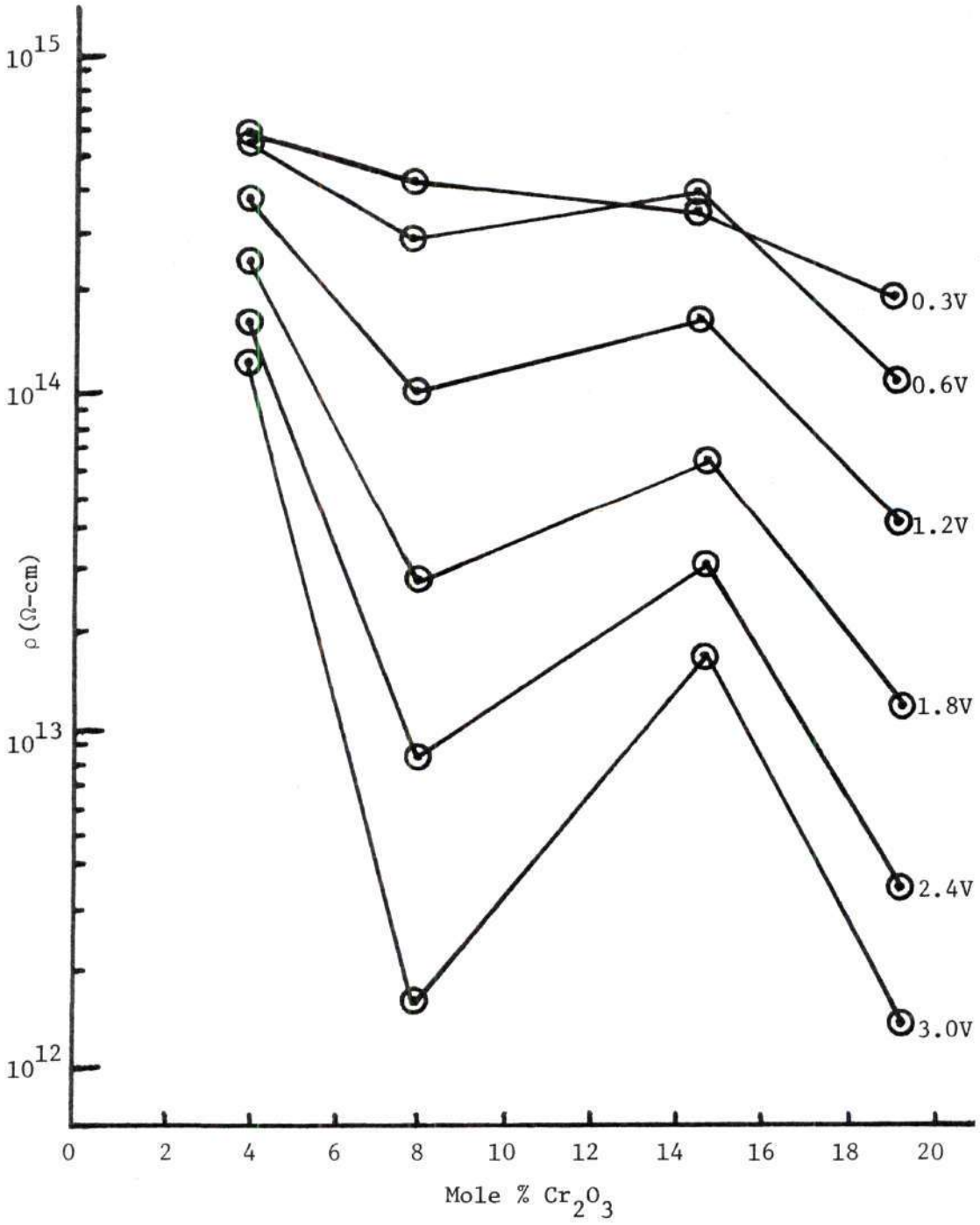

Figure 17. Resistivity As a Function of Mole Percent Cr_2O_3 with Applied Voltage As a Parameter.

each composition varied slightly over two orders of magnitude. In the constant current method, the voltage was limited to a range of 0 to 1 volt, resulting in approximately a one order of magnitude change in average resistivities. Thus, low resistivity measurement are attributed to defects in the films.

A study of the average resistivities, Figure 15, for each film indicates that only an order of magnitude exists between the resistivities of any two compositions. Published works[23-25] on resistivities of bulk Al_2O_3-Cr_2O_3 samples at elevated temperatures (400°C - 1500°C) have all shown a three order of magnitude difference for samples containing 0 to 20 mole percent Cr_2O_3. Extrapolation of Hensler and Henry's data[23] from 600°C to room temperature shows an eight order of magnitude difference between 0 to 20 mole percent Cr_2O_3 in Al_2O_3, Figure 15. Eremenko and Beinish's data[25] extrapolated from 300-400°C to room temperature is also plotted in Figure 15. The resistivity at room temperature for 100 mole percent Al_2O_3 from Salama's data[32] is approximately 5.5×10^{15} ohm-cm and the resistivity at room temperature from Barbe and Herman's data[35] for 100 mole percent Cr_2O_3 is approximately 6.5×10^{9} ohm-cm, a difference of six orders of magnitude between thin films of the pure oxides. If extrapolation of resistivities by the Arrhenius equation from elevated temperatures to room temperature is valid, resistivities of thin $Al_{2-x}Cr_xO_3$ films appear to differ substantially from those of the bulk oxide mixtures. Although nondispersive X-ray traces showed the Cr content in the films to increase with increasing Cr_2O_3 content, this is only a relative measure and the actual composition of the sputtered film could be substantially different from those of the targets,

i.e., preferential sputtering of Al_2O_3 over Cr_2O_3 could have occurred. The actual Cr_2O_3 content would then be small enough so as to not affect resistivity measurements to any great extent, explaining the reason why the average resistivities were all within an order of magnitude of one another. Another possibility is that Cr_2O_3 contents of up to 19.0 mole percent in Al_2O_3 have no effect on the room temperature resisitivity of the sputtered films.

Dielectric Strength

Dielectric strengths for the different mole percent Cr_2O_3 compositions (see Appendix C) indicated that the Cr_2O_3 additions had virtually no effect on the dielectric strength of the Al_2O_3 films. The dielectric strength of the pure Al_2O_3 films agreed well with previous published data (see Survey of the Literature). Average values for the dielectric strength calculated at first sign of breakdown, E_{min}, and at massive film breakdown, E_{max}, are plotted in Figure 18. Either the Cr_2O_3 content is much less in the films than the targets or Cr_2O_3 content up to 19.0 mole percent does not affect dielectric strength significantly.

Two types of dielectric breakdown in insulators under an applied electric field can occur:[12] electronic and thermal. Electronic occurs when a localized voltage gradient reaches some value corresponding to intrinsic electrical breakdown. Thermal breakdown occurs when local overheating causes the local conductivity to increase to a point where instability occurs and permits a rush of current, melting, and puncture. Thermal breakdown appeared to be the dominant mechanism causing the

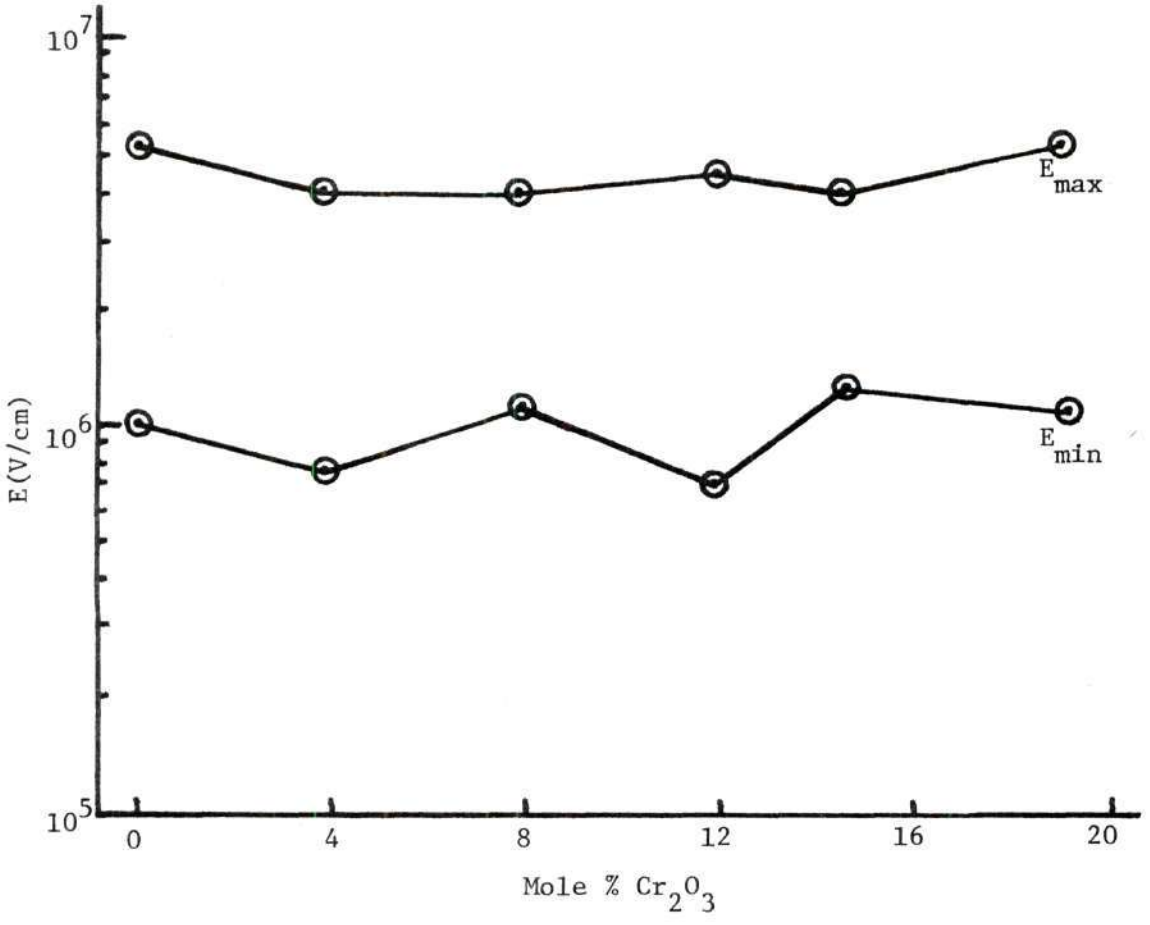

Figure 18. Average Dielectric Strength As a Function of Mole Percent Cr_2O_3.

dielectric failure in the films since film heating was detected. In the 7.8 and 14.6 mole percent composition films, what appeared to be melting or vaporization of the underlying Al film could be seen extending radially outward from the contact area; heating was not quite as noticeable as this in the other compositions. Breakdown was detected visibly by small arcs and propagation of break channels in the film. Massive breakdown was visible as film breakdown extending out away from the top electrode area after a violent arc. Such breakdown is illustrated in Figure 19.

The mode of breakdown was slightly different in the 7.8 and 14.6 mole percent Cr_2O_3 composition films. Closely following what appeared to be melting or vaporization of the underlying Al film, a sudden burst of many tiny arcs was visible, indicating dielectric failure. Further increase of applied voltage created intermittent arcs becoming larger and larger until the film surrounding the electrode was destroyed. In the other compositions, the first sign of breakdown occurred as one or several small arcs, with a fissure-like break in the film under the electrode. Increasing the applied voltage further yielded the same results as in the 7.8 and 14.6 mole percent Cr_2O_3 samples. No explanation for this difference in the initial film breakdown mode could be offered, unless the 7.8 and 14.6 mole percent Cr_2O_3 are more homogeneous with fewer defects.

A small percentage of the samples (2 to 3 percent) exhibited no dielectric failure at the low voltage ranges. The initial dielectric failure at low voltages is further evidence of defects in the films and

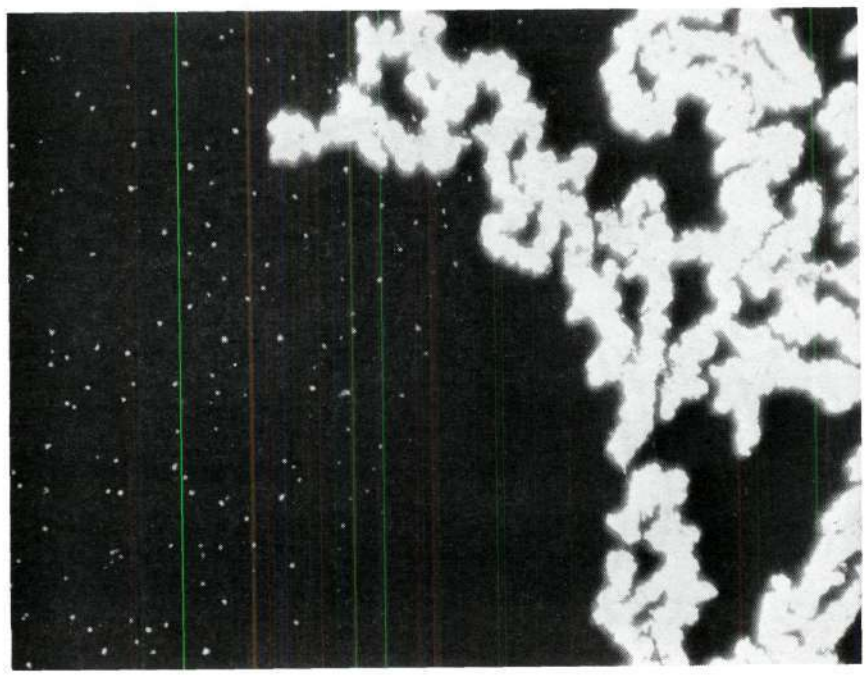

Figure 19. Film Breakdown in Sputtered Film. Transmitted Light, X200.

thus supports the postulation that the large resistivity ranges in some of the films are caused by defects in the films.

CHAPTER V

CONCLUSIONS

1. The average resistivities ($\cong 5 \times 10^{14}$ ohm-cm) of the thin $Al_{2-x}Cr_xO_3$ films sputtered from solid solution targets ranging in composition from 0 to 19.0 mole percent Cr_2O_3 varied approximately one order of magnitude and experimental scatter prevented composition dependence determination.

2. The average dielectric strengths of the thin $Al_{2-x}Cr_xO_3$ films sputtered from targets ranging in composition from 0 to 19.0 mole percent Cr_2O_3 varied approximately one order of magnitude and were not composition dependent.

3. Two types of conduction were identified in the $Al_{2-x}Cr_xO_3$ films:

   a. At low applied fields, films of 4.1 and 19.0 mole percent Cr_2O_3 exhibited ohmic conduction but no evidence of ohmic conduction was found in the 7.8 and 14.6 mole percent Cr_2O_3 films.

   b. At high applied fields, all compositions exhibited conduction that varied exponentially with the square root of the applied electric field.

4. Thin films sputtered from $Al_{2-x}Cr_xO_3$ targets containing up to 19.0 mole percent Cr_2O_3, at temperatures of 350-450^{o}C and deposition rates between 13-42 A/min, have the γ-Al_2O_3 structure.

CHAPTER VI

RECOMMENDATIONS

Increasing mole percent additions of Cr_2O_3 to Al_2O_3 were expected to lower the resisitivity of the r.f. sputtered thin films. The resistivities of the $Al_{2-x}Cr_xO_3$ films containing up to 19.0 mole percent Cr_2O_3 varied approximately one order of magnitude. Further studies should concentrate on resistivity measurements of the $Al_{2-x}Cr_xO_3$ thin films to determine if increasing mole percent additions of Cr_2O_3 does affect the resistivity of the films. Higher mole percent Cr_2O_3 sputtering targets should also be fabricated to investigate the effect of higher mole percent Cr_2O_3 concentrations in the thin films.

BIBLIOGRAPHY

1. Maissel, L. I. and Glang, R., Handbook of Thin Film Technology, McGraw-Hill Book Co., New York, N.Y., 1970, Chapters 3, 4, 14, 19.

2. Vossen, J. L. and O'Neill, J. J., Jr., "R-F Sputtering Processes," RCA Review, 29 [2] 149-79 (June, 1968).

3. Davidse, P. D. and Maissel, L. I., "Dielectric Thin Films Through r. f. Sputtering," Journal of Applied Physics, 37[2] 574-9 (Feb., 1966).

4. Jackson, G. N., "R.f. Sputtering," Thin Solid Films, 5 (1970) 209-46.

5. Wehner, G. K. and Kenknight, C. E. and Rosenberg, D., "Modification of the Lunar Surface by the Solar-Wind Bombardment," Planetary and Space Science, 11 (1963) 1257-61.

6. Pliskin, W. A., "The Evaluation of Thin Film Insulators," Thin Solid Films, 2 (1968) 1-26.

7. Davidse, P. D., "Theory and Practice of RF Sputtering," Symposium on the Deposition of Thin Films by Sputtering, University of Rochester, June 9, 1966, 75-85.

8. MacDonald, R. J. and Haneman, D., "Low-Energy-Ion-Bombardment Damage in Germanium," Journal of Applied Physics, 37 [8] 3048-56 (1966).

9. Wyckoff, R., Crystal Structures, Vol. II, Interscience Publishers, Inc., New York, N.Y., 1948, Chapter V, p. 4.

10. Davey, W., "Precision Measurements of the Crystal Structures of Al_2O_3, Fe_2O_3, and Cr_2O_3," Physical Review, 21 (1963) 716.

11. Lynch, J. and Ruderer, C. and Duckworth, W. (Editors), Engineering Properties of Selected Ceramic Materials, American Ceramic Society, Inc., Columbus, Ohio, 1966, Section 5.4.

12. Kingery, W., Introduction to Ceramics, John Wiley and Sons, Inc., New York, N.Y., 1960, p. 162-3, 665, 732-6.

13. Bunting, E., "Phase Equilibria in the System Cr_2O_3 - Al_2O_3," U.S. Bureau of Standards Journal of Research, 6 [6] 947-9 (1931).

14. Mier, M. and Buvinger, E., "A Comparative Study of Anodized, Evaporated, and Sputtered Aluminum Oxide Thin Films," Journal of Vacuum Science and Technology, 6 [4] 727-30 (1969).

15. Frieser, R., "Phase Changes in Thin Reactively Sputtered Alumina Films," Journal of the Electrochemical Society, 113 [4[357-60 (1966).

16. Pratt, I., "Thin-Film Dielectric Properties of r.f. Sputtered Oxides," Solid State Technology, 12 [1] 49-57 (1969).

17. Salama, C., "RF Sputtered Aluminum Oxide Films on Silicon," Journal of Electrochemical Society, 117 [7] 913-17 (1970).

18. Smith, R., Circuits, Devices and Systems, John Wiley and Sons, Inc., New York, N.Y., 1966, p. 266.

19. Henry, E., Electronic Ceramics, Doubleday and Co., Inc., Garden City, N.Y., 1969, p. 92.

20. Cohen, J., "Electrical Conductivity of Alumina," Bulletin of the American Ceramic Society, 38 [9] 441-6 (1959).

21. Crawford, J. and Vest, R., "Electrical Conductivity of Single-Crystal Cr_2O_3," Journal of Applied Physics, 35 [8[2413-18 (1964).

22. Stone, H., "The Electrical Conductivity of Chromic Oxide in the Range 500° - 1300°C," Materials Science and Engineering, 2 (1967/68) 348-9.

23. Hensler, J. and Henry, E., "Electrical Resistance of Some Refractory Oxides and Their Mixtures in the Temperature Range 600° to 1500°C," Journal of the American Ceramic Society, 36 [3] 76-83 (1953).

24. Vernetti, R. and Cook, R., "Effect of Metal Oxide Additions on the High-Temperature Electrical Conductivity of Alumina," Journal of the American Ceramic Society, 49 [4] 194-9 (1966).

25. Eremenko, V. and Beinish, A., "Electrical Conductivity of Binary Systems Formed by Refractory Oxides," Zhurnal Neorganicheskoi Khimii, 1 [9] 2118-30 (1956).

26. Pratt, I., "Growth and Electrical Characteristics of r.f. Sputtered Aluminum Oxide," Thin Solid Films, 3 (1969) R23-R26.

27. Salama, C., "RF Sputtered Aluminum Oxide Films on Silicon," Solid State Science, 117 [7] 913-7 (1970).

28. Tanaka, T. and Iwauchi, S., "The Characteristics of Al-Al_2O_3-Si Structures Formed by Reactive Sputtering," Japanese Journal of Applied Physics, 7 (1968) 1420.

29. Ryabova, L. and Savitskaya, Ya., "The Preparation of Thin Films of Some Oxides by the Pyrolysis Method," Thin Solid Films, 2 (1968) 141-8.

30. Lamb, D., Electrical Conduction Mechanisms in Thin Insulating Films, Methuen and Co. LTD., London, 1967.

31. Emtage, P. and Tantraporn, W., "Schottky Emission through Thin Insulating Films," Physical Review Letters, 8 [7] 267-8 (1962).

32. Salama, C., "Conduction in Al_2O_3 Films and Charge Storage in MAOS Structures," Journal of the Electrochemical Society, 118 [2] 1993-8 (1971).

33. Mead, C., "Electron Transport Mechanisms in Thin Insulating Films," Physical Review, 128 [5] 2088-93 (1962).

34. Thilo, E., Jander, J. and Seemann, H., "Die Farbe des Rubins und der $(Al,Cr)_2O_3$ - Mischkristalle," Zeitschrift fur anorganische und allgemeine Chemie, 279 (1955) 2-17.

35. Barbe, D. and Herman, D., "Transport Processes in Amorphous Cr_2O_3 Films," Journal of Applied Physics, 41 [7] 3116-20 (1970).

APPENDICES

APPENDIX A

CRYSTAL STRUCTURE AND COMPOSITION MEASUREMENT

Solid Solution Determination

As mentioned previously, powder X-ray diffraction was used as the method to determine whether the fired sputter targets had assumed a complete solid solution. Since α-Al_2O_3 and Cr_2O_3 belong to the same crystallographic class, the same reflections for each compound on an X-ray diffraction pattern will be close together, separated only by several degrees due to different lattice spacings existing in each compound. This separation is more than adequate to cause separate and distinct peaks to be present on the diffraction pattern of an unfired mixture of the two oxides, as is the case for the unfired 20 mole percent Cr_2O_3 in Al_2O_3 sample, Figure 20. In a solid solution of the two oxides, no such separation of peaks should be evident, shown clearly by the reflections for the fired 20 mole percent Cr_2O_3 in Al_2O_3 sample superimposed over the same reflections for the unfired samples, Figure 20. Since all of the fired compositions indicated no separation of peaks in their respective X-ray patterns, it was concluded that all of the fired samples existed in complete solid solution.

Target Composition Determination

X-ray fluorescence was used as the method to determine fired target compositions. Powdered samples of both the unfired (standards) and fired compositions (unknowns) were pressed uniaxially in a small

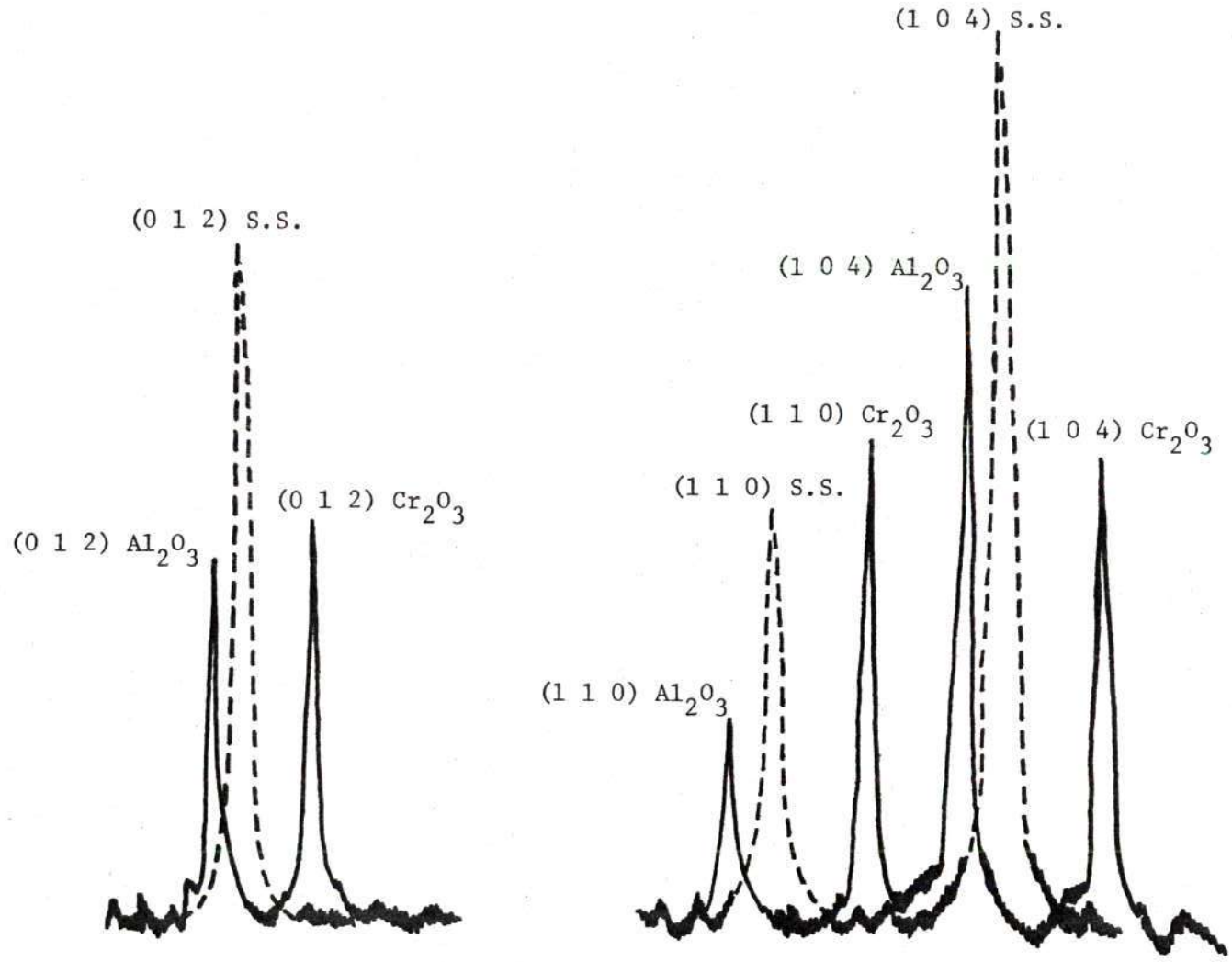

Figure 20. Difference in X-ray Diffraction Patterns for a 20 Mole Percent Cr_2O_3 in Al_2O_3 Sample Which Is Unfired (Solid Lines) and Fired to Form a Solid Solution (Dotted Lines).

hydraulic hand press to pellets 1-1/4 inch in diameter at a pressure of approximately 8000 psi. The goniometer on the X-ray fluorescent unit was set at an angle, $2\theta = 69.33^{o}$, such that the scintillation counter could pick up counts from the characteristic chromium peak for Cu Kα radiation. After the samples had been placed under vacuum ($< 200\ \mu$), the surface of each sample was bombarded with high intensity X-rays with the subsequent X-ray counts received being recorded for 100 second time intervals, Table 11. Graphing the results for the standards, Figure 21, enabled the unknown compositions to be obtained by matching counts with the corresponding composition.

Table 11. X-Ray Fluorescent Data

Set No.	Counts for Standards				
	4% Cr_2O_3	8% Cr_2O_3	12.5% Cr_2O_3	16% Cr_2O_3	20% Cr_2O_3
1	404718	787118	905509	1444906	1723213
2	405463	786672	907873	1444427	1727759
3	405154	786955	908836	1447109	1725419
Average	405112	786915	907406	1445481	1725464

Set No.	Counts for Unknowns				
	A	B	C	D	E
1	418089	778529	1121144	1334879	1668210
2	417283	777122	1119099	1345364	1669100
3	416395	776956	1116587	1340930	1665552
Average	417256	777536	1118943	1340391	1667621

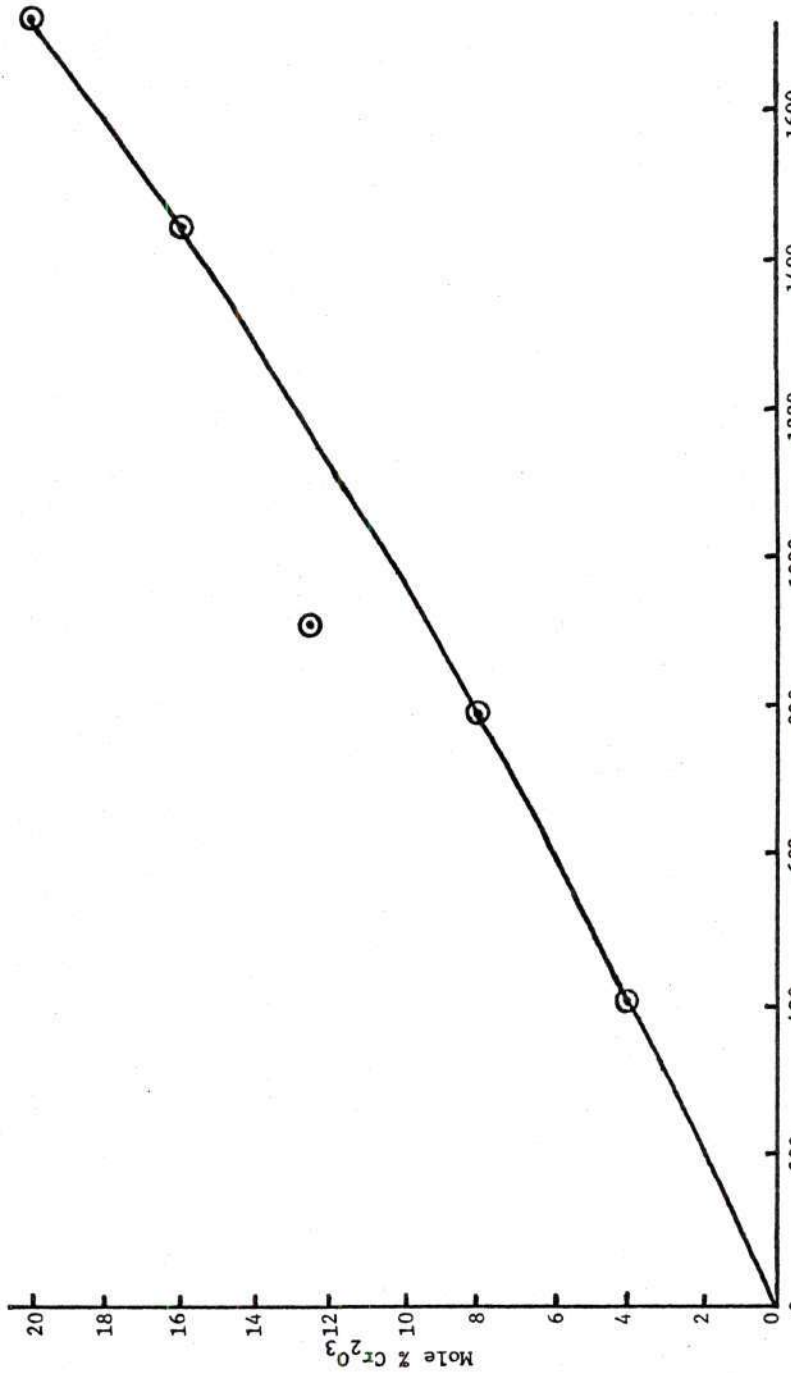

Figure 21. Number of Chromium Counts in Various Cr_2O_3-Al_2O_3 Mole Percent Mixtures.

APPENDIX B

RESISTIVITIES

The following table lists the resistivity values for the sputtered films calculated using the formula

$$\rho = \frac{RA}{t}$$

where

ρ = resistivity in ohm-centimeters,

R = resistance in ohms,

A = area in square centimeters, and

t = thickness in centimeters.

Table 12. Resistivities for the Sputtered Films

Composition (mole % Cr_2O_3)	Sample No.	ρ (Ω-cm)	Composition (mole % Cr_2O_3)	Sample No.	ρ (Ω-cm)
0	40-43.1	2.39×10^{13}	4.1	40-59.2	1.09×10^{15}
		3.17×10^{13}			1.13×10^{15}
		2.61×10^{13}			4.86×10^{14}
		3.17×10^{13}			7.70×10^{13}
		4.73×10^{13}			8.51×10^{13}
		3.23×10^{13}			6.89×10^{14}
		2.11×10^{14}			4.46×10^{13}
		2.17×10^{14}		40-60.1	2.19×10^{15}
		2.22×10^{14}			3.17×10^{12}
		1.78×10^{13}			2.01×10^{13}
	40-43.2	4.08×10^{14}			2.77×10^{13}
		3.95×10^{13}			2.19×10^{13}
		4.86×10^{14}			3.52×10^{13}
		2.52×10^{14}			1.03×10^{15}
		2.20×10^{13}			1.56×10^{15}
		4.40×10^{13}			1.87×10^{15}
		9.06×10^{14}			1.52×10^{15}
				40-60.2	2.20×10^{15}
					2.37×10^{15}
4.1	40-59.1	1.53×10^{15}			1.04×10^{14}
		1.04×10^{15}			2.16×10^{14}
		3.41×10^{14}			2.76×10^{13}
		5.43×10^{14}			1.81×10^{13}
		8.39×10^{14}			2.50×10^{13}
		3.46×10^{14}			1.64×10^{15}
		3.95×10^{14}			1.04×10^{13}
		6.42×10^{14}		40-61.1	4.20×10^{14}
		1.14×10^{14}			8.01×10^{13}

Table 12. Resistivities for the Sputtered Films (Contd.)

Composition (mole % Cr_2O_3)	Sample No.	ρ (Ω-cm)
4.1	40-61.1	8.78×10^{13}
		5.34×10^{13}
		7.63×10^{14}
		3.43×10^{14}
		4.20×10^{14}
	40-61.2	1.00×10^{15}
		8.90×10^{14}
		4.08×10^{14}
		5.93×10^{14}
		2.56×10^{14}
		4.82×10^{14}
		6.30×10^{14}
		3.08×10^{13}
		1.48×10^{15}
		1.00×10^{15}
7.8	40-53.1	2.03×10^{15}
		1.14×10^{13}
		1.04×10^{15}
		9.93×10^{14}
		3.88×10^{15}
		8.51×10^{14}
		8.04×10^{14}
		9.46×10^{14}
		8.51×10^{12}
		2.84×10^{14}
7.8	40-53.2	1.43×10^{15}
		1.76×10^{14}
		4.39×10^{14}
		2.01×10^{13}
		8.05×10^{12}
		1.35×10^{13}
		5.49×10^{11}
		1.06×10^{15}
	40-54.1	8.78×10^{14}
		2.30×10^{13}
		8.41×10^{13}
		5.85×10^{14}
		1.02×10^{13}
		2.12×10^{13}
	40-54.2	1.31×10^{11}
		3.20×10^{13}
	40-55.1	1.45×10^{10}
		1.28×10^{10}
		2.90×10^{12}
		6.20×10^{11}
		1.32×10^{15}
		1.16×10^{14}
	40-55.2	3.42×10^{14}
		4.70×10^{12}
		5.12×10^{10}
		1.84×10^{13}
		8.11×10^{11}

Table 12. Resistivities for the Sputtered Films (Contd.)

Composition (mole % Cr_2O_3)	Sample No.	ρ (Ω-cm)
7.8	40-55.2	2.95×10^{13}
11.8	40-45.1	2.53×10^{13}
		2.69×10^{11}
		3.42×10^{12}
		4.79×10^{12}
		2.90×10^{13}
		3.95×10^{11}
	40-45.2	2.48×10^{14}
		3.42×10^{13}
		2.11×10^{15}
		2.63×10^{14}
		2.21×10^{11}
	40-46.1	6.24×10^{7}
		8.66×10^{7}
	40-46.2	1.32×10^{10}
		9.72×10^{7}
		2.19×10^{7}
		1.10×10^{11}
		2.48×10^{10}
		1.47×10^{10}
	40-47.1	1.16×10^{9}
		3.21×10^{9}
	40-47.2	4.96×10^{7}
		5.42×10^{7}
		3.25×10^{8}
11.8	40-47.2	9.48×10^{7}
		6.77×10^{7}
		1.53×10^{8}
	40-49.1	2.00×10^{11}
14.6	40-56.1	6.91×10^{14}
		1.34×10^{14}
		7.34×10^{14}
		1.51×10^{14}
		1.60×10^{15}
		9.06×10^{14}
		3.45×10^{14}
		1.38×10^{14}
		7.34×10^{13}
	40-56.2	8.60×10^{14}
		3.68×10^{14}
		2.66×10^{13}
		1.15×10^{14}
		4.91×10^{14}
		8.60×10^{13}
		2.70×10^{13}
		5.73×10^{14}
		2.46×10^{14}
	40-57.1	1.52×10^{15}
		6.47×10^{9}
		4.62×10^{13}

Table 12. Resistivities for the Sputtered Films (Contd.)

Composition (mole % Cr_2O_3)	Sample No.	ρ (Ω-cm)
14.6	40-57.1	2.12×10^{14}
		3.00×10^{14}
		1.80×10^{14}
		1.71×10^{14}
		7.85×10^{13}
		8.78×10^{14}
	40-57.2	1.51×10^{15}
		9.24×10^{14}
		6.72×10^{13}
		2.52×10^{14}
		9.66×10^{14}
		2.94×10^{10}
		1.13×10^{14}
	40-58.1	1.85×10^{15}
		2.67×10^{15}
		1.09×10^{15}
		1.20×10^{15}
		7.63×10^{14}
		1.14×10^{15}
		3.81×10^{11}
		2.34×10^{15}
	40-58.2	1.91×10^{15}
		1.76×10^{15}
		8.26×10^{14}
		9.81×10^{14}
		8.78×10^{12}
		4.13×10^{14}

Composition (mole % Cr_2O_3)	Sample No.	ρ (Ω-cm)
14.6	40-58.2	8.26×10^{15}
		2.79×10^{15}
19.0	40-50.1	3.77×10^{12}
		2.40×10^{11}
		1.64×10^{13}
		2.97×10^{13}
		1.60×10^{12}
		2.08×10^{13}
		1.55×10^{14}
		3.28×10^{11}
	40-50.2	2.16×10^{13}
		3.33×10^{13}
		2.16×10^{13}
		1.91×10^{13}
		6.65×10^{13}
		3.45×10^{13}
		6.24×10^{9}
		2.83×10^{13}
		2.74×10^{13}
	40-51.1	3.07×10^{13}
		3.59×10^{13}
		4.18×10^{13}
		9.79×10^{14}
		2.55×10^{13}
		3.40×10^{13}

Table 12. Resistivities for the Sputtered Films (Contd.)

Composition (mole % Cr_2O_3)	Sample No.	ρ (Ω-cm)	Composition (mole % Cr_2O_3)	Sample No.	ρ (Ω-cm)
19.0	40-51.1	2.42×10^{13}	19.0	40-52.1	4.37×10^{13}
		3.72×10^{13}			9.52×10^{14}
	40-51.2	3.18×10^{13}			1.01×10^{15}
		3.38×10^{13}			7.28×10^{14}
		8.28×10^{13}			2.13×10^{10}
		1.08×10^{12}		40-52.2	1.68×10^{15}
		3.50×10^{13}			8.71×10^{14}
		5.16×10^{13}			1.63×10^{15}
		3.76×10^{13}			1.86×10^{15}
		3.12×10^{13}			2.96×10^{13}
	40-52.1	1.06×10^{15}			1.57×10^{15}
		6.16×10^{14}			1.22×10^{15}
		8.40×10^{14}			1.51×10^{15}
		4.93×10^{13}			1.74×10^{15}
		6.16×10^{14}			

APPENDIX C

DIELECTRIC STRENGTHS

Dielectric strengths, calculated using the formula

$$E = \frac{V_B}{d}$$

where

E = dielectric strength in volts/cm,

V_B = breakdown voltage in volts, and

d = sputtered film thickness in cm,

are listed in Table 13. The dielectric strength at first sign of film breakdown is listed as E_{min} and the dielectric strength at massive film breakdown is listed as E_{max}.

Table 13. Dielectric Strengths of the Sputtered Films

Composition (mole % Cr_2O_3)	Sample No.	$E_{min}x10^{-5}$ (V/cm)	$E_{max}x10^{-6}$ (V/cm)	Composition (mole % Cr_2O_3)	Sample No.	$E_{min}x10^{-5}$ (V/cm)	$E_{max}10^{-6}$ (V/cm)
0	40-43.1	7.75	4.86	4.1	40-59.2	7.69	5.64
		14.1	5.56			7.18	4.87
		12.7	4.45		40-60.1	4.63	5.48
		6.06	5.07			12.4	5.14
		8.45	4.15			6.78	4.97
		9.15	5.84			15.8	4.80
		10.6	5.21			5.08	4.74
		13.4	4.22		40-60.2	7.10	3.99
		11.3	6.69			5.03	4.15
		12.0	4.58			9.29	4.26
	40-43.2	7.95	5.41		40-61.1	18.4	3.09
		11.5	6.64			6.76	3.00
		10.6	5.41			4.54	4.01
		9.02	5.57			4.44	3.62
		9.84	5.34			6.28	2.95
		10.6	5.90		40-61.2	7.04	3.29
		13.1	8.20			5.16	3.19
						5.63	3.10
						4.41	3.24
4.1	40-59.1	9.38	4.88			11.3	3.47
		4.38	5.18				
		8.12	4.75				
		7.50	4.19	7.8	40-53.1	12.0	4.91
		8.75	5.19			11.4	5.93
	40-59.2	13.3	4.05			10.2	6.59
		5.13	4.62			7.18	4.49
		10.2	4.51			10.8	4.61

Table 13. Dielectric Strengths of the Sputtered Films (Contd.)

Composition (mole % Cr_2O_3)	Sample No.	$E_{min} \times 10^{-5}$ (V/cm)	$E_{max} \times 10^{-6}$ (V/cm)	Composition (mole % Cr_2O_3)	Sample No.	$E_{min} \times 10^{-5}$ (V/cm)	$E_{max} \times 10^{-6}$ (V/cm)
7.8	40-53.2	5.56	3.89	11.8	40-45.2	6.00	6.67
		11.1	4.44			5.60	5.47
		12.5	4.44		40-46.1	12.7	4.38
		6.48	3.94		40-46.2	5.56	3.10
		13.9	6.02			5.15	3.49
	40-54.1	13.9	3.70			4.36	2.78
		7.87	4.17			3.97	2.46
		10.6	3.75			6.75	3.06
		8.33	3.94		40-47.1	9.33	5.13
		13.0	3.61		40-47.2	8.00	4.80
	40-54.2	17.0	3.13			12.6	6.28
		5.53	3.69			14.8	4.91
		15.7	2.86			13.1	4.00
		12.4	3.22			7.43	5.20
		14.7	3.59		40-49.1	27.4	6.03
	40-55.1	20.9	4.29				
		16.8	3.04				
	40-55.2	9.73	3.68	14.6	40-56.1	10.4	4.26
		12.4	3.89			7.65	3.93
						5.24	4.10
						12.0	4.75
11.8	40-45.1	4.00	3.60			15.3	4.00
		6.27	5.33		40-56.2	13.5	4.04
		5.33	4.67			4.77	3.52
		6.67	5.53			3.94	3.32
		7.33	5.13			4.14	4.46
	40-45.2	8.67	7.33			7.25	3.94

Table 13. Dielectric Strengths of the Sputtered Films (Contd.)

Composition (mole % Cr_2O_3)	Sample No.	$E_{min}x10^{-5}$ (V/cm)	$E_{max}x10^{-6}$ (V/cm)	Composition (mole % Cr_2O_3)	Sample No.	$E_{min}x10^{-5}$ (V/cm)	$E_{max}x10^{-6}$ (V/cm)
14.6	40-57.1	18.1	4.68	19.0	40-50.1	14.6	5.17
		13.4	4.15			8.43	4.55
		15.2	4.33		40-50.2	4.42	3.89
		15.2	4.04			6.84	5.26
		14.6	3.39			8.42	4.74
	40-57.2	13.3	3.83			7.89	4.52
		19.1	4.26		40-51.1	12.4	6.20
		5.32	3.72			6.94	5.12
		13.8	3.30			12.4	6.61
		13.3	4.36			22.3	6.45
	40-58.1	14.5	4.76			13.2	6.12
		15.9	5.03		40-51.2	12.9	6.77
		15.9	6.21			9.68	6.94
		16.6	4.55			7.74	6.77
		23.4	4.48			13.7	6.61
	40-58.2	17.0	4.64			7.42	7.42
		16.3	4.31		40-52.1	12.8	6.52
		17.0	4.12			12.0	7.09
		17.0	4.18			8.51	5.89
		13.7	5.36			20.6	7.09
						10.6	5.67
					40-52.2	11.0	7.20
19.0	40-50.1	7.86	4.44			18.4	6.25
		4.72	3.82			25.0	8.09
		7.30	4.38				

APPENDIX D

CURRENT-VOLTAGE RELATIONSHIPS

Current-voltage relationships were studied in terms of the square root of the applied field versus the current density. The applied field was obtained using the equation

$$E = \frac{V}{d}$$

where

E = applied field in volts/cm,

V = applied voltage in volts, and

d = thickness of the sputtered film in cm.

Current densities were obtained using the equation

$$J = \frac{I}{A}$$

where

J = current density in amperes/cm^2,

I = current in amperes, and

A = area of the electrode in cm^2.

Table 14 lists the calculated values.

Table 14. $\sqrt{E}$ and Current Densities for the Sputtered Films

Composition (mole % Cr_2O_3)	Sample No.	$\sqrt{E} \times 10^{-2}$ ($[V/cm]^{1/2}$)	$J \times 10^{9}$ (A/cm^2)	Composition (mole % Cr_2O_3)	Sample No.	$\sqrt{E} \times 10^{-2}$ ($[V/cm]^{1/2}$)	$J \times 10^{9}$ (A/cm^2)
4.1	40-59.1	1.37	0.027	4.1	40-60.1	3.44	38.0
		1.94	0.047			3.68	120.0
		2.37	0.087			3.90	278.0
		2.74	0.101			4.12	392.0
		3.06	0.108		40-60.2	1.28	0.291
		3.35	0.152			1.81	0.481
		3.62	0.215			2.22	0.633
		3.87	0.266			2.56	1.07
		4.11	0.380			2.86	2.28
		4.33	0.519			3.14	11.4
	40-59.2	1.24	0.018			3.39	55.7
		1.75	0.032			3.62	190.0
		2.15	0.051			3.84	316.0
		2.48	0.076			4.05	456.0
		2.77	0.104		40-61.1	1.20	0.020
		3.04	0.177			1.70	0.037
		3.28	0.253			2.08	0.076
		3.51	0.316			2.41	0.139
		3.72	0.367			2.69	0.266
		3.92	0.443			2.95	0.570
	40-60.1	1.30	0.506			3.18	1.26
		1.84	0.911			3.40	2.66
		2.25	1.39			3.61	4.56
		2.60	2.53			3.81	6.46
		2.91	4.68		40-61.2	1.19	0.016
		3.19	9.87			1.68	0.052

Table 14. $\sqrt{E}$ and Current Densities for the Sputtered Films (Contd.)

Composition (mole % Cr_2O_3)	Sample No.	$\sqrt{E} \times 10^{-2}$ ($[V/cm]^{1/2}$)	$J \times 10^{9}$ (A/cm^2)	Composition (mole % Cr_2O_3)	Sample No.	$\sqrt{E} \times 10^{-2}$ ($[V/cm]^{1/2}$)	$J \times 10^{9}$ (A/cm^2)
4.1	40-61.2	2.06	0.105	7.8	40-53.2	3.33	46.8
		2.37	0.202			3.54	74.7
		2.65	0.430			3.73	418.0
		2.91	0.785		40-54.1	1.18	0.015
		3.14	1.26			1.67	0.042
		3.36	2.28			2.04	0.076
		3.56	3.67			2.36	0.190
		3.75	9.11			2.64	0.418
						2.89	1.11
						3.12	2.78
7.8	40-53.1	1.34	0.418			3.33	6.58
		1.90	0.848			3.54	15.2
		2.32	2.53			3.73	31.6
		2.68	7.34		40-55.1	1.25	0.022
		3.00	20.2			1.77	0.086
		3.28	44.3			2.17	0.316
		3.55	83.5			2.51	0.987
		3.79	139.0			2.80	2.40
		4.02	190.0			3.07	3.92
		4.24	253.0			3.32	7.34
	40-53.2	1.18	0.709			3.54	11.6
		1.67	1.77			3.76	31.6
		2.04	2.91			3.96	595.0
		2.36	9.75				
		2.64	12.6				
		2.89	20.2				
		3.12	31.6	14.6	40-56.1	1.28	0.062

Table 14. $\sqrt{E}$ and Current Densities for the Sputtered Films (Contd.)

Composition (mole % Cr_2O_3)	Sample No.	$\sqrt{E} \times 10^{-2}$ ($[V/cm]^{1/2}$)	$J \times 10^{9}$ (A/cm^2)	Composition (mole % Cr_2O_3)	Sample No.	$\sqrt{E} \times 10^{-2}$ ($[V/cm]^{1/2}$)	$J \times 10^{9}$ (A/cm^2)
14.6	40-56.1	1.81	0.086	14.6	40-57.1	3.97	12.2
		2.22	0.126			4.19	22.8
		2.56	0.266		40-57.2	1.26	0.029
		2.86	0.354			1.79	0.038
		3.14	0.481			2.19	0.108
		3.39	0.709			2.53	0.253
		3.62	1.05			2.82	0.772
		3.84	1.64			3.09	2.02
		4.05	2.28			3.34	4.81
	40-56.2	1.25	0.047			3.57	10.9
		1.76	0.228			3.79	29.1
		2.16	0.797			3.99	72.2
		2.49	2.40		40-58.1	1.44	0.126
		2.79	5.19			2.03	0.342
		3.05	9.62			2.49	0.861
		3.30	16.4			2.88	1.90
		3.56	25.3			3.22	3.80
		3.74	36.7			3.52	7.09
		3.94	50.6			3.80	11.6
	40-57.1	1.32	0.034			4.07	19.0
		1.87	0.051			4.32	25.3
		2.29	0.095			4.55	35.4
		2.65	0.240		40-58.2	1.40	0.085
		2.96	0.608			1.98	0.164
		3.24	1.52			2.42	0.304
		3.50	3.04			2.80	0.582
		3.75	6.33			3.13	1.39

Table 14. $\sqrt{E}$ and Current Densities for the Sputtered Films (Contd.)

Composition (mole % Cr_2O_3)	Sample No.	$\sqrt{E} \times 10^{-2}$ ($[V/cm]^{1/2}$)	$J \times 10^{9}$ (A/cm^2)	Composition (mole % Cr_2O_3)	Sample No.	$\sqrt{E} \times 10^{-2}$ ($[V/cm]^{1/2}$)	$J \times 10^{9}$ (A/cm^2)
14.6	40-58.2	3.43	3.42	19.0	40-51.1	1.57	0.047
		3.70	7.22			2.23	0.126
		3.96	13.9			2.73	0.342
		4.20	18.9			3.15	0.734
		4.43	32.9			3.52	1.77
						3.86	4.18
						4.16	11.3
19.0	40-50.1	1.30	0.316			4.45	29.1
		1.84	0.797			4.72	73.4
		2.25	1.52		40-51.2	1.56	0.038
		2.60	2.66			2.20	0.278
		2.90	3.92			2.69	0.671
		3.18	6.58			3.11	1.39
		3.43	10.8			3.48	3.04
		3.67	20.2			3.81	5.82
		3.89	36.7			4.12	12.6
		4.10	75.9			4.40	30.4
	40-50.2	1.26	0.053			4.67	75.9
		1.78	0.190			4.92	152.0
		2.18	0.468		40-52.1	1.46	0.734
		2.51	1.18			2.06	1.90
		2.81	3.67			2.53	3.92
		3.08	16.4			2.92	6.33
		3.32	58.2			3.26	10.6
		3.55	164.0			3.57	20.2
		3.77	266.0			3.86	30.4
		3.97	367.0			4.12	46.8

Table 14. $\sqrt{E}$ and Current Densities for the Sputtered Films

Composition (mole % Cr_2O_3)	Sample No.	$\sqrt{E} \times 10^{-2}$ ($[V/cm]^{1/2}$)	$J \times 10^{9}$ (A/cm^2)	Composition (mole % Cr_2O_3)	Sample No.	$\sqrt{E} \times 10^{-2}$ ($[V/cm]^{1/2}$)	$J \times 10^{9}$ (A/cm^2)
19.0	40-52.1	4.38	68.4	19.0	40-52.2	3.32	21.5
		4.61	93.7			3.63	22.8
	40-52.2	1.48	0.899			3.93	26.6
		2.10	1.64			4.20	38.0
		2.57	2.91			4.46	65.8
		2.97	4.18			4.70	122.0

APPENDIX E

LATTICE PARAMETER DETERMINATION

To determine lattice parameters from electron diffraction patterns, a scope constant was calculated based on a MgO standard and the equation

$$K = Rd \tag{8}$$

where

K = scope constant,

R = radius of hkℓ reflection, and

d = d-spacing of hkℓ reflection.

After solving for K, d-spacings of the thin film compositions were calculated. Calculated d-spacings for the 7.8, 11.8 and 19.0 mole percent Cr_2O_3 films matched closely with those of γ-Al_2O_3. Since γ-Al_2O_3 is in the cubic system, only one lattice parameter exists since a = b = c and it can be calculated using

$$a^2 = d^2(h^2 + k^2 + \ell^2) \tag{9}$$

where

a = lattice parameter,

d = d-spacing, and

h, k, ℓ = Miller indices of a specific reflection.

Calculated lattice parameters for the 7.8, 11.8 and 19.0 mole percent Cr_2O_3 films are listed in Table 15.

Table 15. Lattice Parameters for 7.8, 11.8 and 19.0 Mole Percent Cr_2O_3 Films

Composition (Mole % Cr_2O_3)	Calculated d-spacing (A)	d-spacing for γ-Al_2O_3 (A)	hkℓ Reflection	Lattice Parameter, a (A)
7.8	1.9803	1.977	400	7.9212
	1.3994	1.395	440	7.916
	1.1534	1.140	444	7.9910
	0.9629	0.989	800	7.7032
	0.8464	0.884	840	7.5704
	0.7833	0.806	844	7.6747
11.8	1.9867	1.977	400	7.9468
	1.4537	1.395	440	8.2279
	1.2163	1.140	444	8.4290
	0.9386	0.989	800	7.5088
	0.8701	0.884	840	7.7787
19.0	1.9803	1.977	400	7.9212
	1.3810	1.395	440	7.8121
	1.1534	1.140	444	7.9910
	0.9901	0.989	800	7.9208
	0.8895	0.884	840	7.9559
	0.8074	0.806	844	7.9109